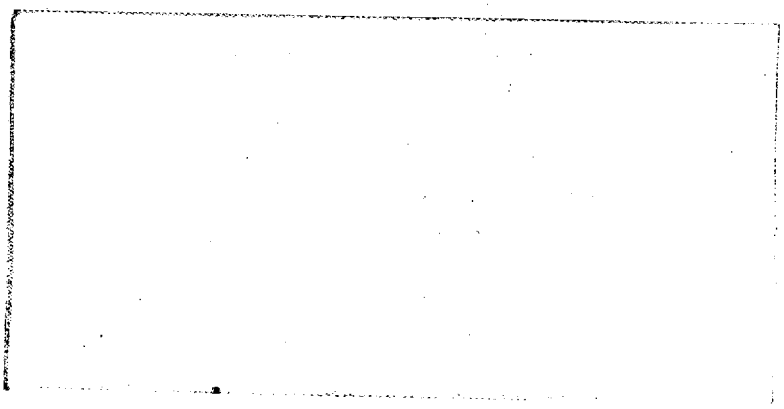

STATINTL

[redacted]

#5

REPORT 974-013-2

FINAL REPORT ON THE DESIGN, CONSTRUCTION, AND TESTING OF A LIQUID BEARING INCORPORATING A BUILT-IN PUMP

September 1965

STATINTL

[redacted]

974-013-2

FOREWORD

STATINTL

[redacted] submits this report in compliance with Part II of the Contract Brief of Contract No. [redacted] STATINTL

Approved

Research Manager

ABSTRACT

The purpose of this assignment was to design, construct and test a liquid bearing of a design different from the pressure plenum type employed previously. The bearing which is self powered and incorporates its own fluid pump, was built and some of the testing conducted in the first phase of the program under Contract No. [redacted] as described in Report No. 974-013-1. This report, which describes the final tests carried out on this bearing, also summarizes the earlier program for convenience.

Due to the allocation of priorities to other assignments, time did not permit testing of other configurations or the design and testing of a prototype bearing complete with drive motor and controls based on the results of this program, however, a production illustration showing this idealized design is included.

STATINTL

CONTENTS

CONTENTS (continued)

ILLUSTRATIONS

ILLUSTRATIONS (continued)

1. INTRODUCTION

The self-powered liquid bearing design, which is fully described in Report 974-013-1, was developed to overcome inefficiencies in the pressure plenum type of liquid bearing, and the losses associated with the isolated pumps, piping and hardware required to energize them.*

This phase of the program was conducted to complete tests required to determine the most efficient configuration for the impeller "cage" or load bearing surface. The tests described in this report were outstanding from the preceding contract, and are those considered as being essential to a final evaluation of the design concept.

2. SUMMARY OF PRECEDING TEST PROGRAM

To assist in the appreciation of the program as a whole, tests conducted in the first phase of the program and described in Report 974-013-1, are summarized below.

2.1 PHYSICAL DESCRIPTION

The prototype Rotatron bearing is a squirrel-cage axial-vane pump, 4-inches in diameter, with 12 blades set at 30 degrees from the radial (Figure 1). The pump was caged, in the first series of tests, in a helix of 1/8-inch diameter wire, one-half of which is left-hand wound, and the other right-hand wound. Approximately 120 degrees of the circumference of the undersurface was covered by a plate which extended for the whole length of the blades. This cage, and the slotted and perforated cages, rested in contoured cradles on a mounting plate, thus making it possible to rotate them through 360 degrees, if required (Figure 2).

2.2 TEST FACILITY

To provide a suitable test facility, a special tank was constructed, approximately 24-inches square by 42-inches deep (Figure 3). Water level in the tank permitted covering of the bearing to a depth of approximately 4-inches. Tank capacity at this level was 104 gallons. The test drive system consisted of a 1/3-horsepower electric motor driving the final drive shaft through "V" belts, various pulleys (four in the system) and a 2 to 1 ratio speed reducer. The rotatron was connected to the drive shaft by a rubber flexible coupling (Figure 4).

STATINTL *Reference [redacted] Report 974-001 measuring the pressure drop across standard P.V.C. fittings.

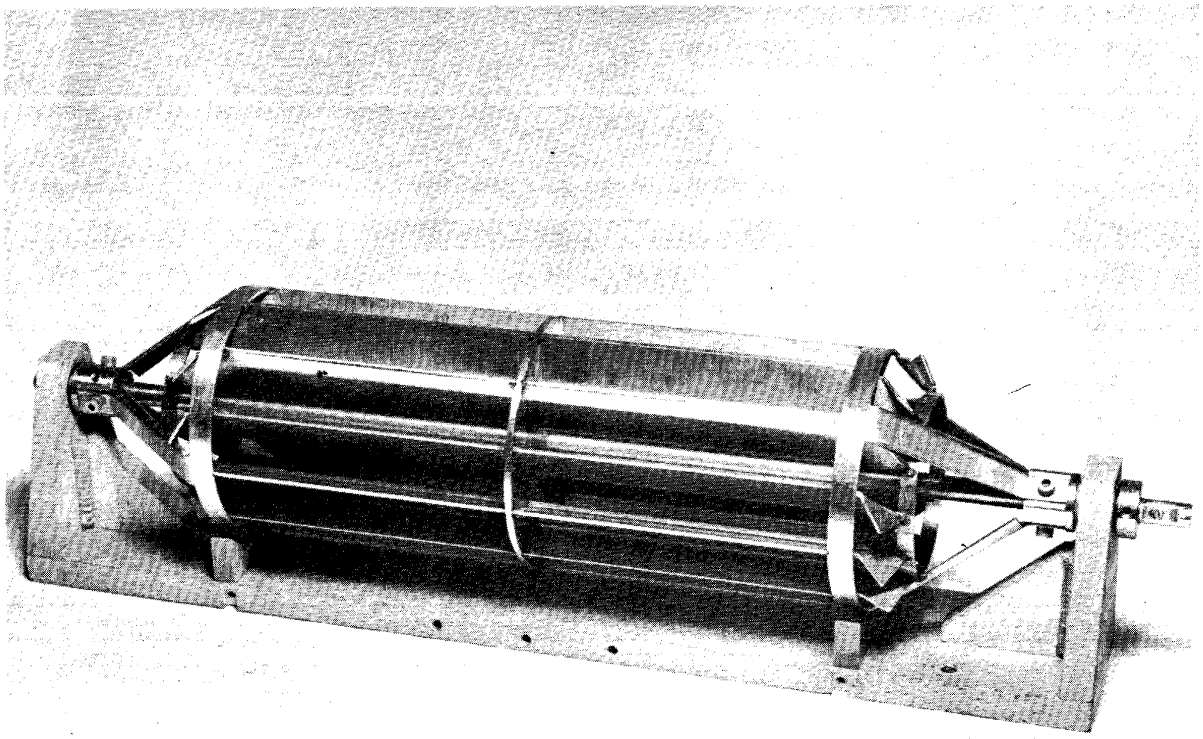

974-013-2

Figure 1. Rotatron Impeller

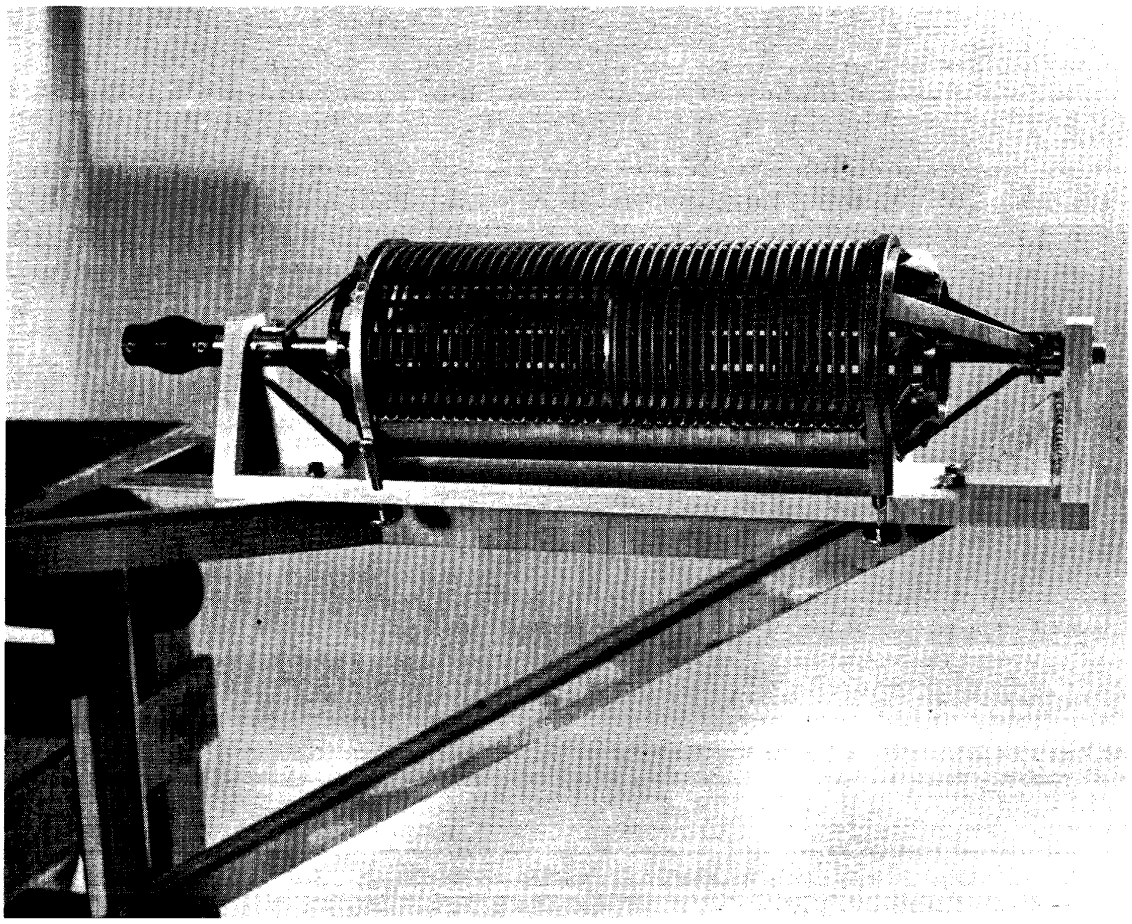

Figure 2. Rotatron on Test Tank Support

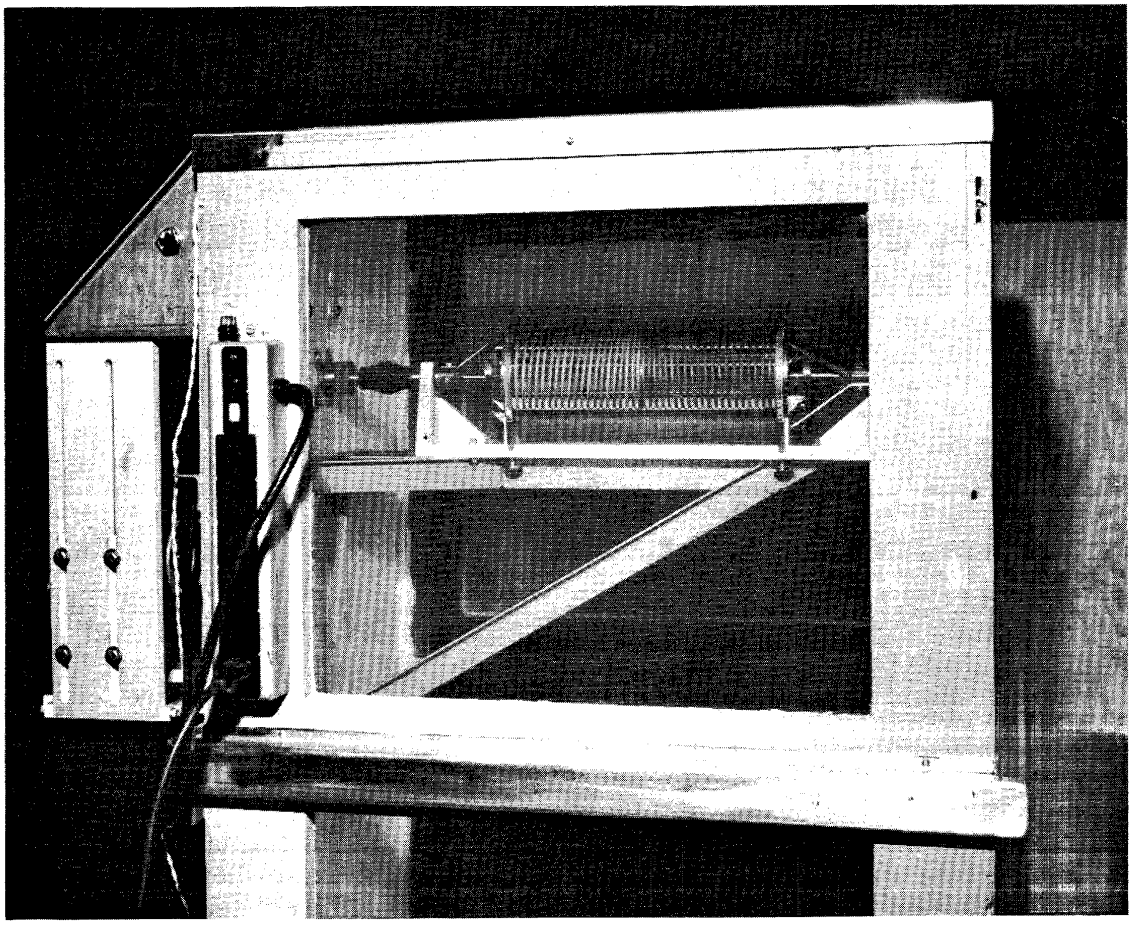

Figure 3. Rotatron In Test Tank

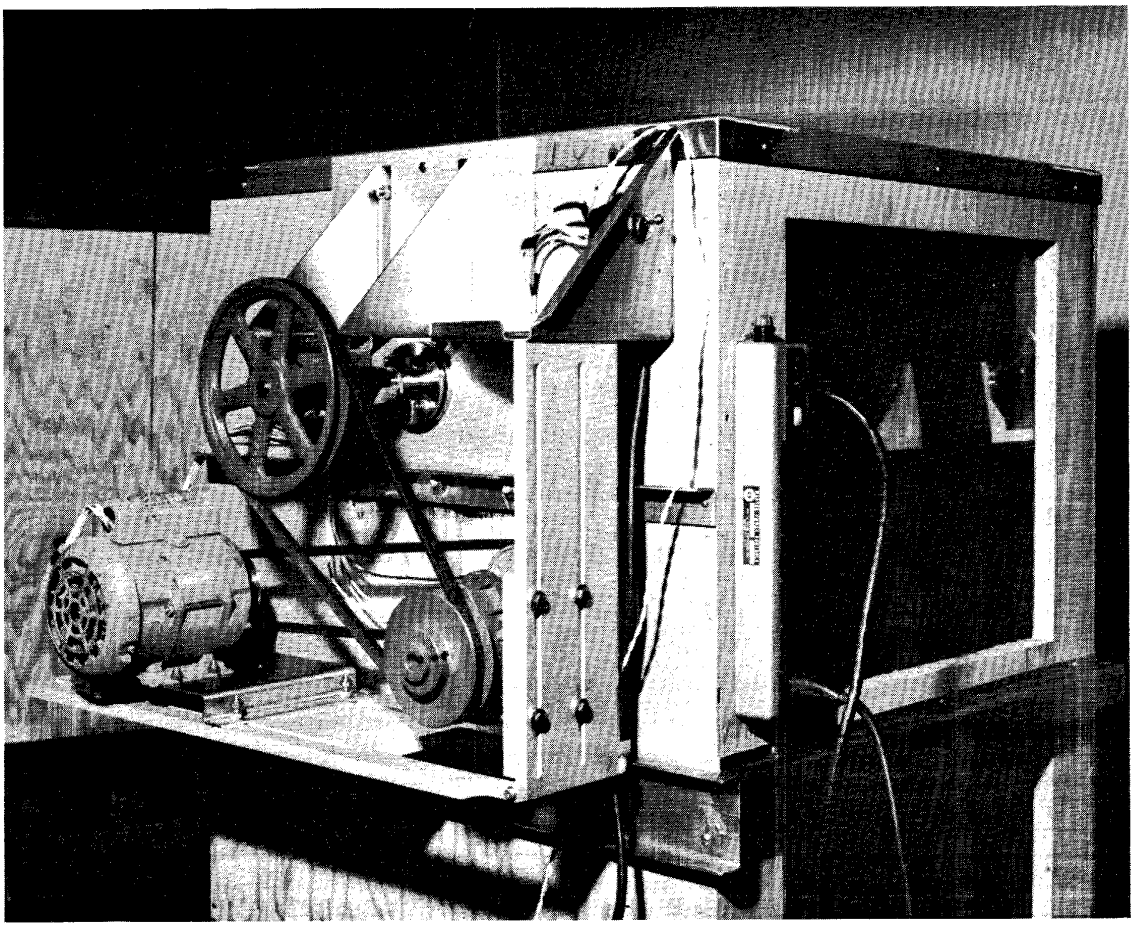

Figure 4. Drive System

2.3 TESTS AND RESULTS

2.3.1. Rotatron without Film.

The first tests were run without film to study the flow pattern. A speed of 445 rpm was employed.

2.3.2 Rotatron with Film Loop.

The bearing was next operated at low speeds using a 9-1/2-inch wide loop of thin base mylar leader to determine the effect of speed on load supporting capability. A load of 1-1/2 pounds was placed in the film loop by means of a loaded regulation spool. An adequate support cushion was formed at 150 rpm, but the loop immediately moved off center. The helix cage used in this test was designed on the basis that the helixes would tend to direct the fluid to converge in the center of the bearing, thereby centering the film. It was obvious from this test that the helix concept (Figure 5) was not effective.

2.3.3. Bearing Shape versus Film Tracking.

The impeller was designed to provide a pressure build-up in the center which would result in a "crown" effect of solution over the surface of the bearing somewhat analoguous to that of a crowned belt pulley, except that the film slid off the crown. To provide a valley, or trough, in which the film would center, and to decrease the pressure build up, a girdle of perforated aluminum sheet (Figure 6) was wrapped around the center of the cage.* At a speed of 275 rpm, a satisfactory cushion was obtained but further shaping of the girdle and restriction of flow from the center was necessary before a stable cushion exhibiting a self-centering tendency was obtained. The flow pattern can be seen in Figure 7.

2.3.4. Film Transport Assist.

Note was made of the tendency of the film loop to travel in the direction of pump rotation during the testing. The attempt to self-center the film due to vector flow control through the helical cage was not considered entirely satisfactory although indications were that, with a separate development program, thus would be within the realm of possibility.

2.3.5. Fluid Dynamics Reaction.

The next stages of the test program were concerned with reducing the cushion depth to obtain a more stable cushion. The cushion depth was decreased to 3/8-inch at the top by reducing the speed to 150 rpm. The result of this was to cause the film to undulate at an average rate of approximately 60 cps. An increase in the load to 4-pounds necessitated running the bearing at 185 rpm to restore the cushion depth. This change, however, did not cause the undulation to stop. Further test experimenting with damping proved to be effective in conjunction with an increase

STATINTL * Reference [redacted] - Hydromatic Liquid Bearing Assessment.

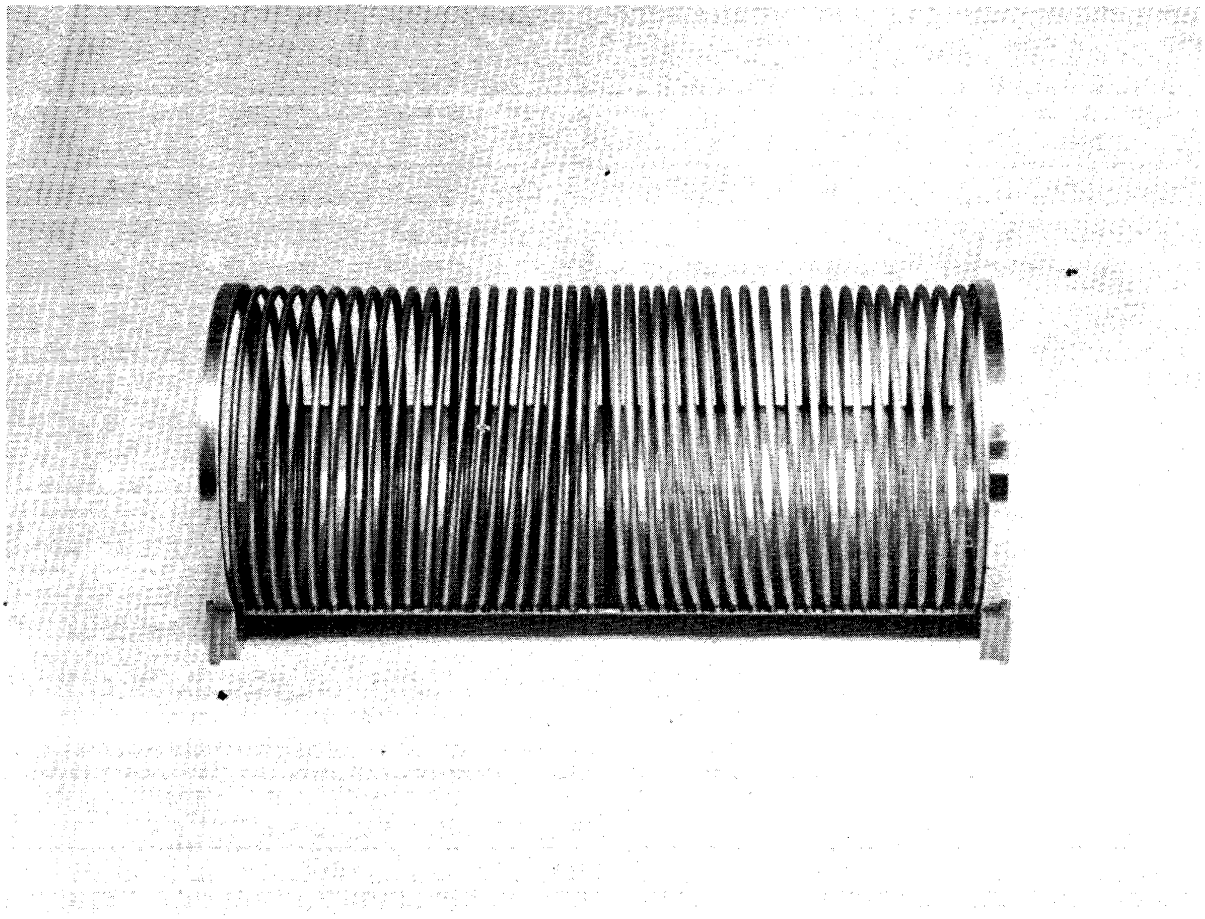

Figure 5. Helix Cage

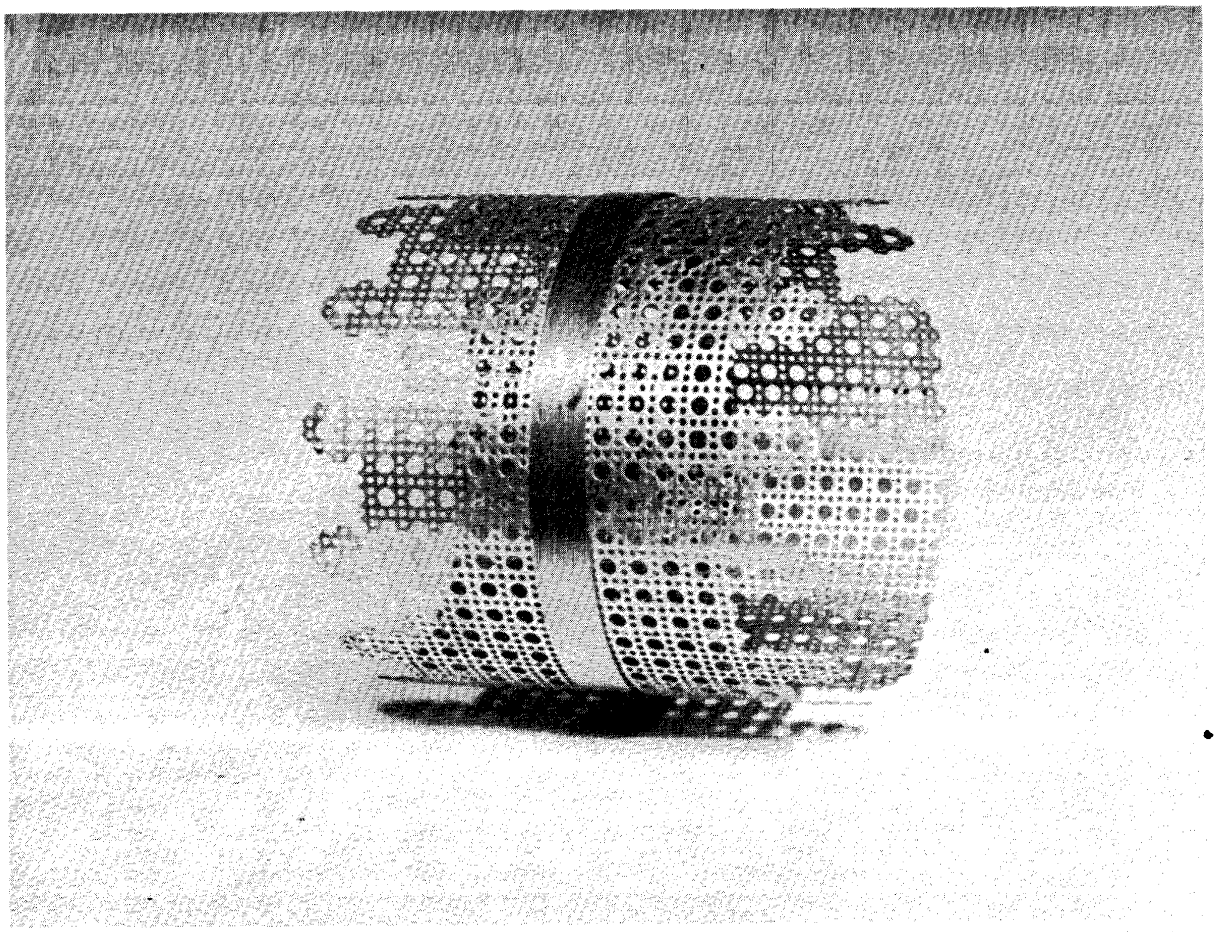

Figure 6. Girdle

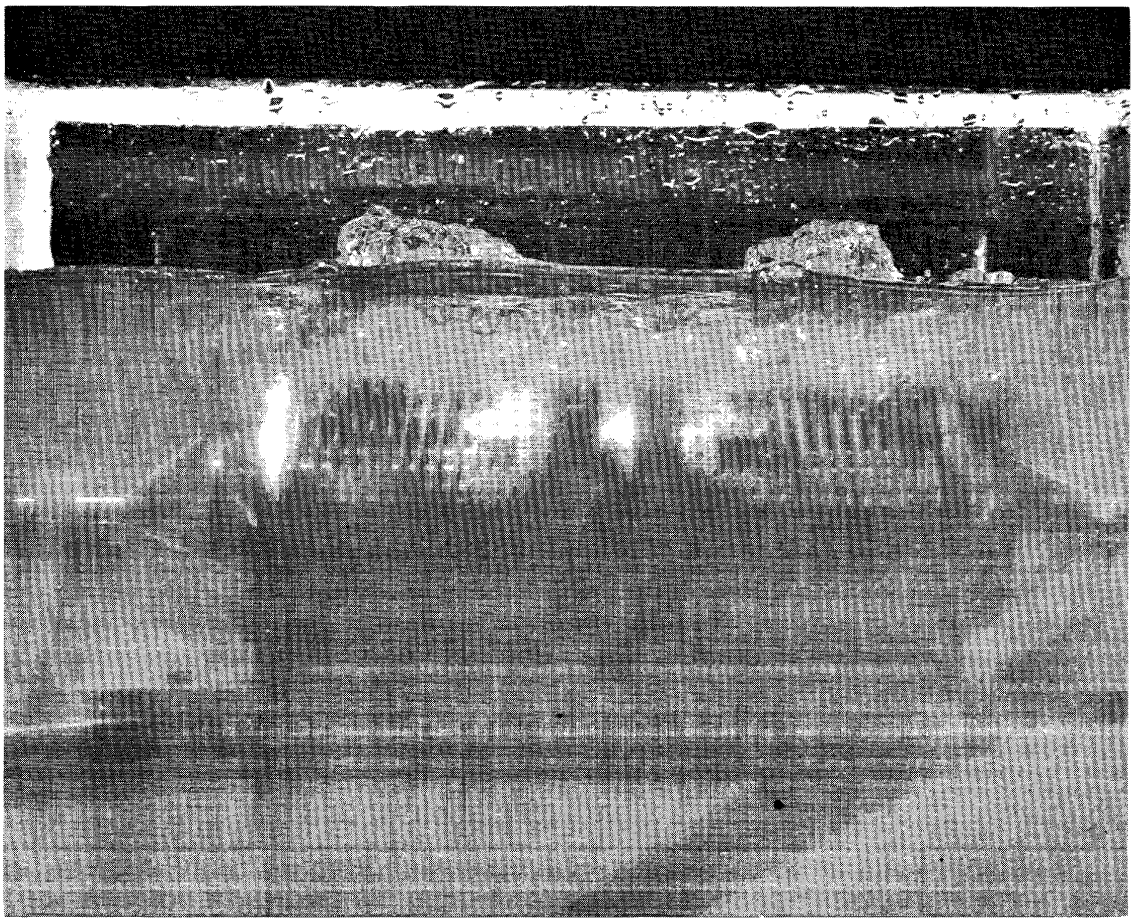

Figure 7. Girdled Helix Flow Pattern

in speed to 250 rpm and rotation of the cage to ensure concentricity of the film loop about the bearing.

2.3.6. Pressure Distribution.
To determine if uneven fluid pressure distribution was responsible for the behavior idiosychrasies of the bearing, a plastic canopy was fabricated (Figure 8). The inside surface simulated a 9-1/2-inch wide film loop on a 7/32-inch depth of cushion. Test runs were made at speeds of 296, 356 and 420 rpm with no girdle, and at 420 rpm with the girdle in place. Evaluation of the pressure plots showed that the impeller operated at a relatively high efficiency. The pressure plots may be found in Appendix A of Report 974-013-1.

2.3.7. Horsepower Requirements.
Further tests were conducted to determine the horsepower requirements of the Rotatron bearing, a flow test encasement was made from plastic tubing (Figure 9). The results of these tests and observations on bearing loads and design parameters have been included as Appendix A of this report.

3. CONTINUATION OF TEST PROGRAM

In this phase of the program, three different configurations of cages were tested, two slotted cages and a cage fabricated from perforated sheeting. The objective was to determine the most efficient method of generating and sustaining a support cushion.

3.1. EVALUATION OF ACRYLIC PLASTIC SLOTTED CAGE

A bearing cage was manufactured from a 4-1/2-inch outside diameter acrylic plastic tube with a wall thickness of 1/8-inch. Fluid outlets were provided in the form of 24 slots of 1/32-inch width, cut through the wall of the tube. The slots were evenly spaced at 15 degrees around the circumference as shown in Figure 10 and cut tangentially to the inside diameters. To reduce the pressure build-up in the center of the cage, a solid section, or island, 1-1/2-inches in length was left in the center of alternate slots.

3.1.1. Test Procedure.
A test was made of the cage performance, using a 9-1/2-inch film loop with an immersed load of 1-1/2-pounds, with the impeller operating at a speed of 267 rpm. A cushion approximately 5/8-inch in depth was formed. The cushion, however, was unstable in that the film rode off the center of the bearing, indicating that the pressure build-up in the center was still forming a "crown" off which the film slid, as observed in previous experiments.

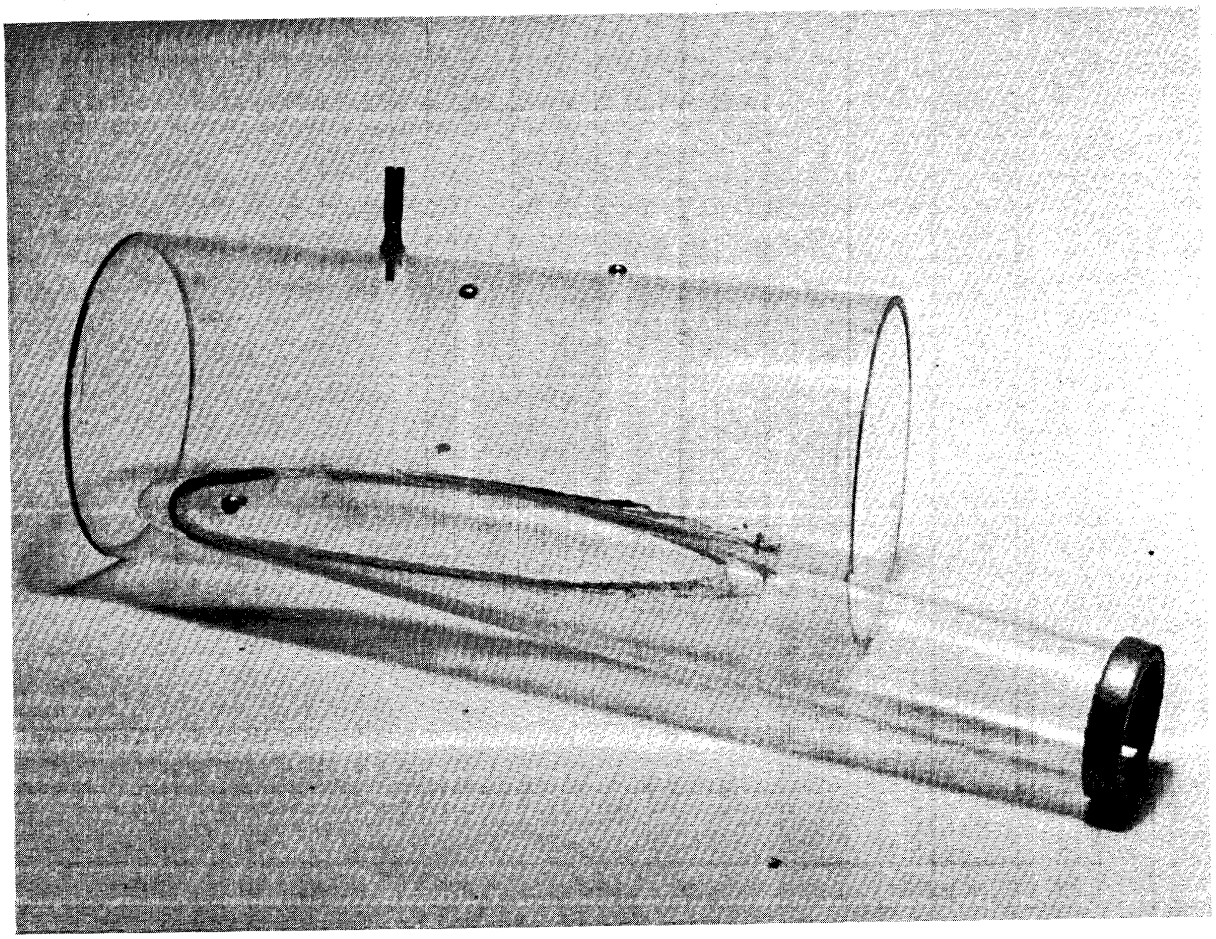

Figure 9. Flow Test Incasement

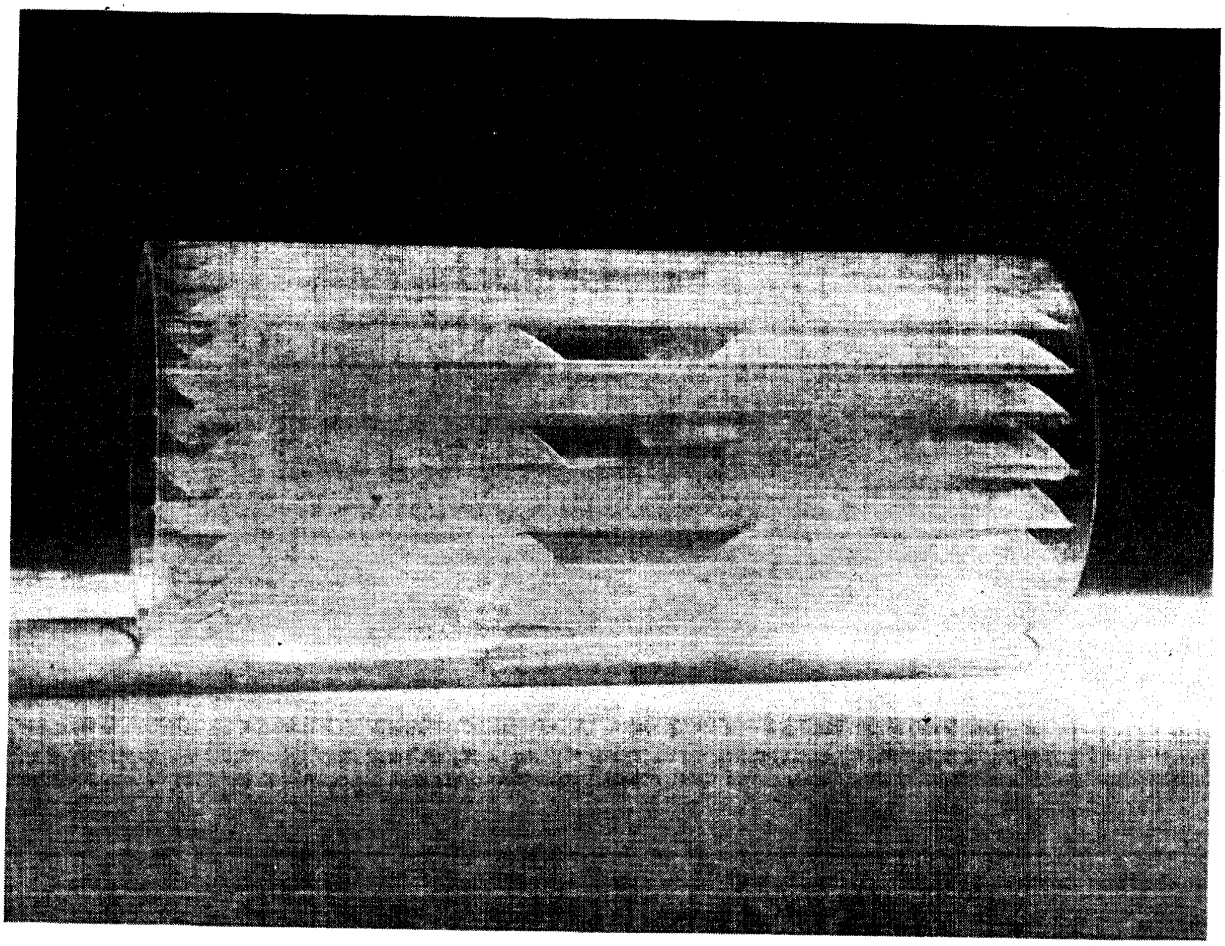

Figure 10. Acrylic Plastic Slotted Cage

During the filling of the test tank with water prior to the above test, and with the bearing in operation, a pronounced clockwise flow was observed over the surface of the bearing cage, indicating that an assist to film transport could be obtained from this configuration of cage. This capability however was not pursued to obtain any relative data.

Based on previous experiments that showed that the higher the film was lifted above the cage surface, the more unstable the support became, a further test was made at a lower impeller speed of 230 rpm to reduce the depth of the cushion. A 3/8-inch cushion was produced, which was more stable and with less tendency for the film to "slide" off the center. Greater stability was obtained when the film was restrained from sideways movement by the addition of a clip at each end of the bearing. Tendency of the film to be driven over the bearing by the fluid flow was again noted.

To determine if the performance of the bearing was repeated with a narrower width of film, a test was conducted using a loop of 5-inch film. The most stable cushion was formed at an impeller speed of 157 rpm with an immersed load of 1-1/4-pounds. A cushion of approximately 1/8-inch was formed, but this was not concentric about the cage circumference. The maximum side cushion was formed at the 8 o'clock station* with little or no cushion at the 4 o'clock station. A strong flow of liquid was observed passing under the lower surface of the bearing cage in the direction of pump rotation. This flow created a negative pressure on the film loop at the 4 o'clock station, and an increased lift at the 8 o'clock station (Figure 11, Sketch A).

To divert the fluid flow below the cage, the space between the cage and the bearing frame on the right-hand side of the bearing was filled in (Figure 11, Sketch B) with the impeller operating again at 157 rpm with the same 5-inch film loop and 1-1/4-pound load, an improvement was noted in concentricity of the film loop, although eccentricity was still present Figure 11, Sketch C. The cushion depth was approximately 1/8-inch from the 10 o'clock to 3 o'clock stations. To decrease the cushion between the 6.30 and 8.30 o'clock area, the slots in this area were taped over. To check the results over a wider area of the bearing, a loop of 6-6-inch film was employed. To reproduce the cushion depth of the previous test, a load of 3-1/4-pounds at an impeller speed of 297 rpm was necessary. The cushion depth at the 8 o'clock was decreased, a retention of the fat cushion was observed below this station, indicating that a flow of liquid persisted below the undersurface of the bearing cage. To further restrict this flow, a perforated screen was added to the left-hand side of the bearing from the 8 o'clock station down to the mounting frame (Figure 11, Sketch D). In this con-

*All stations references are identified from the outboard end of the bearing.

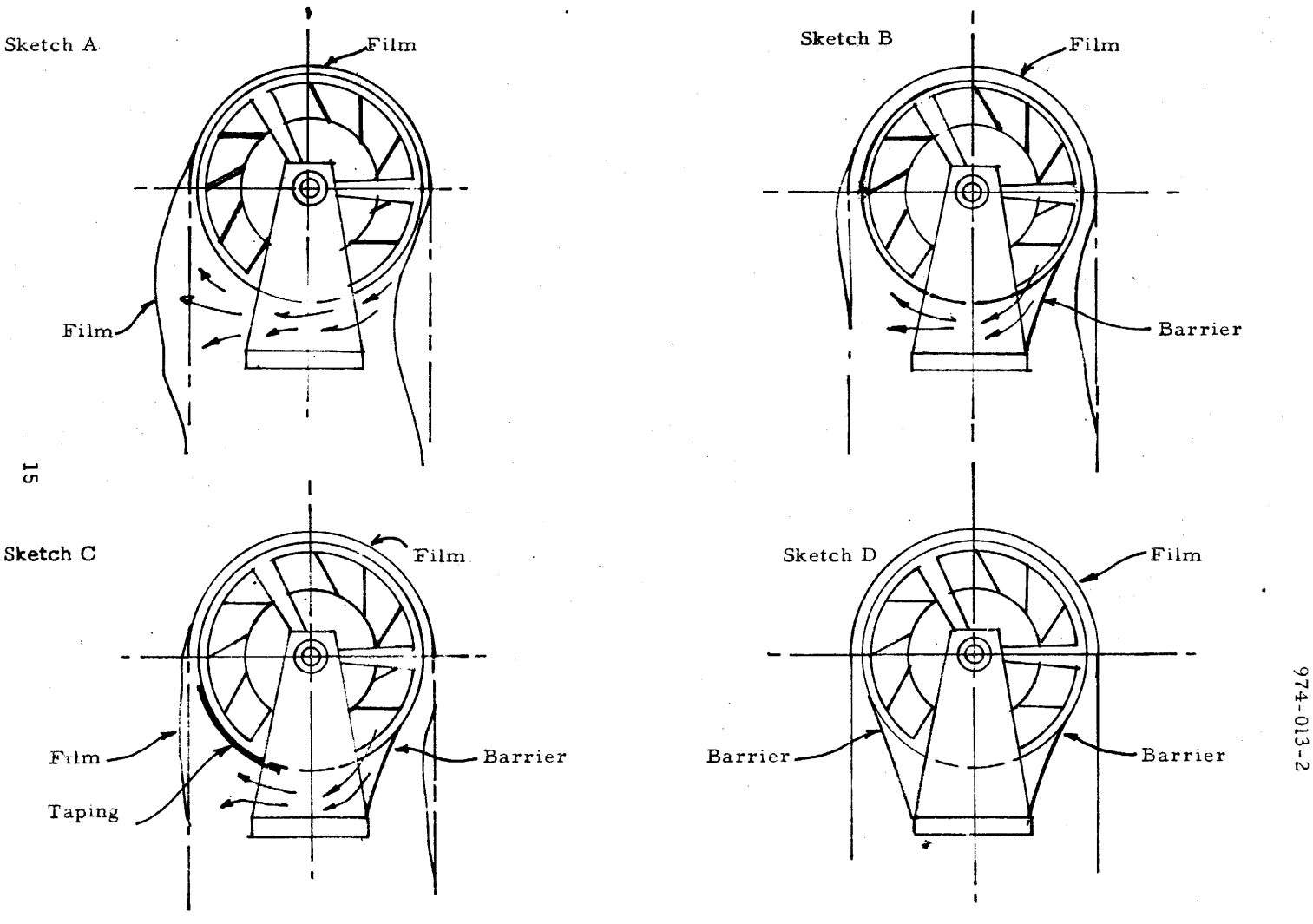

FIGURE 11 Stages in reaching a concentric cushion

figuration the bearing was tested using both 9-1/2-inch and 6.6-inch wide film loops, at an impeller speed of 297 rpm with immersed loads up to 3-1/2-pounds. A concentric film loop was obtained. With the obtaining of a concentric film pass over the bearing, a return was made to the problem of self-centering of the film on the bearing.

Previous experiments conducted to determine methods of hydrodynamic self-centering of the film, showed that the formation of a pressure profile over the 180-degrees surface of the bearing in the shape of a valley rather than a crown was effective. To decrease the existing pressure crown effect in the center of the bearing, a 1/2-inch wide hose clamp was positioned on the center line of the bearing, and tightened to close all the slots about this area. (Figure 12). The bearing was then operated with, 5, 6-6 and 9-1/2-inch widths of film loops. To produce a cushion of approximately 1/8-inch depth it was necessary to increase the bearing speed to 350 rpm. In general, the two narrower widths of film tracked satisfactorily. The 9-1/2-inch film showed a tendency to drift from one side to the other off center, but was prevented from doing so by the addition of a clip on each end of the bearing.

3.2 EVALUATION OF P.V.C. SLOTTED CAGE

This cage was manufactured from a 4-1/2-inch outside diameter P.V.C. tube, with a wall thickness of 1/4-inch. The only difference between this cage and the acrylic plastic cage, was that the inside diameter of the latter provided an 1/8-inch clearance between the inside diameter and the impeller blades. Less than 1/64-inch clearance was obtained with this cage. The objective of the following tests was to determine what, if any, effect the clearance between the blades and the cage had on bearing performance.

3.2.1. Test Procedure.

Test runs were conducted to check this hypothesis. At comparable speeds, the flow through the slots was observed to be similar to that through the unrestricted slots in the acrylic plastic slotted cage, and all widths of film tracked well. The 9-1/2-inch film required the edge restrainers, as it did in the previous tests. The main difference of note in performance of this cage was that with no annular space between the impeller and the cage to form a stable liquid plenum, a wave form was generated in the cushion that resulted in ripples in the film loop which traveled in the direction of the impeller rotation. It was not possible to observe whether this was due to flexing of the cage, or was due to the absence of the dampening effect obtained from a liquid plenum.

In summation, since the traveling wave form in the film loop only occurred in the P.V.C. cage, it is believed that in the design of this

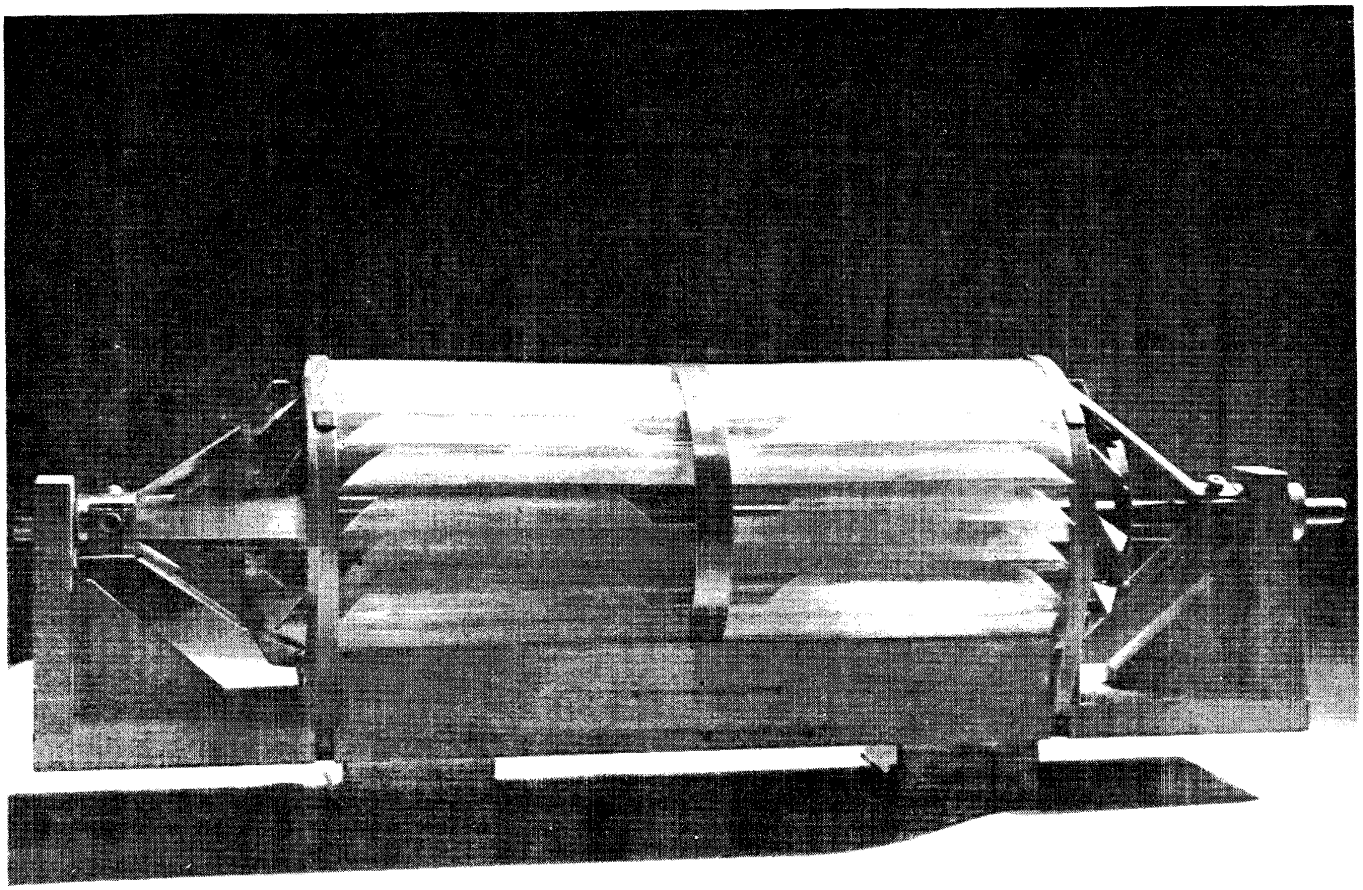

Figure 12. Closing of Sleeve Cage

Approved For Release 2001/09/03 : CIA-RDP78B04747A002800050001-6

type of bearing an annular spacing between the impeller blades and the cage is desirable to provide a margin of safety.

3.3. EVALUATION OF PERFORATED CAGE

On the basis of an analysis of the performance of wire-wound and slotted cages, a perforated screen cage was manufactured from thin perforated aluminum sheeting, rolled to form a cylinder 4-1/2-inches in diameter, and 10-5/8-inches in length (Figure 13). The seam joint was spot welded. The holes in the screen were .041-inches in diameter and were calculated to constitute an open area of 29.7 percent of the bearing cage surface. The cage was assembled on the bearing with the seam at the 6 o'clock undersurface station, to eliminate the effect of the welds. The inside diameter of the cage is 4-15/32-inches, thereby providing a desirable annular spacing of 15/64-inch between it and the impeller (Figure 14).

3.3.1. Test Procedure.

Previous experiments with the impeller demonstrated that the "crown" effect produced was undesirable for centering of the film. For the series of tests with this cage it was decided to restrict the pressure build-up by wrapping the impeller with wire of 1/32-inch diameter for a distance of 1/2-inch each side of the bearing center line. (Figure 15).

On the first test run of the bearing no improvement was noted. To further restrict the pressure build-up at the center disc of the impeller a 1-3/4-inch length of the same material as the cage, was wrapped around the impeller each side of the wire wrapping (Figure 16). The bearing was test run with three film widths and whilst an increase in the valley profile was gained, it was insufficient to cause a marked improvement in self-centering of the film loops.

With the restriction in flow caused by the wrapping of the impeller a decrease in efficiency was apparent, for example, where previously a speed of 150 rpm would be adequate, an rpm of 300 would now be required to obtain the same performance.

To obtain a significant improvement in the valley profile, a further restriction to flow was introduced by the addition of two-1/2-inch widths of tape wrapped around each 1-3/4-inch length of perforated screen.

With the addition of increasing restrictions to flow, in the center of the bearing, the radial flow of fluid from the impeller has been changed considerably, in that a decrease in static head has occurred together with an increase in turbulence resulting in a less stable cushion. Other

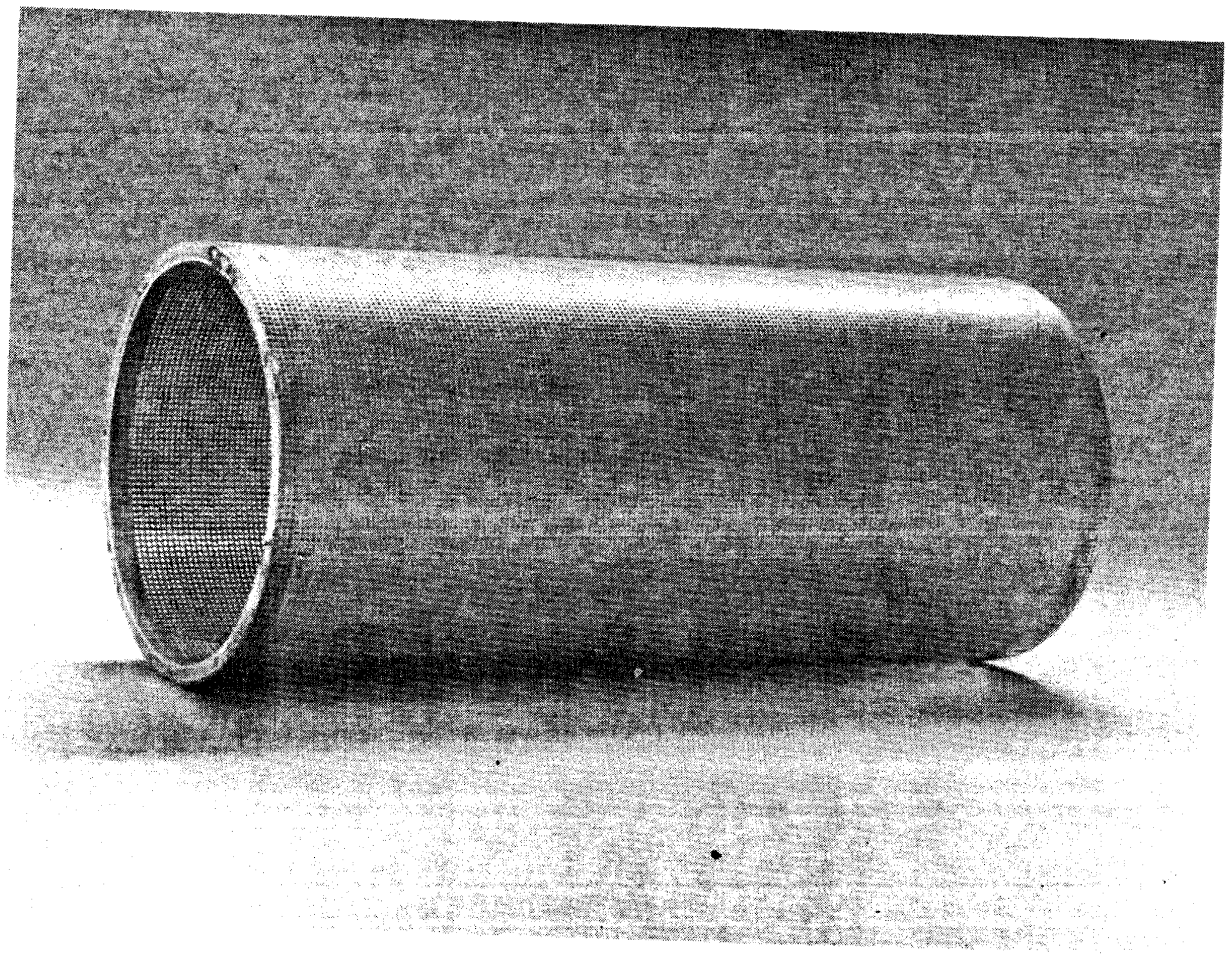

Figure 13. Perforated Cage

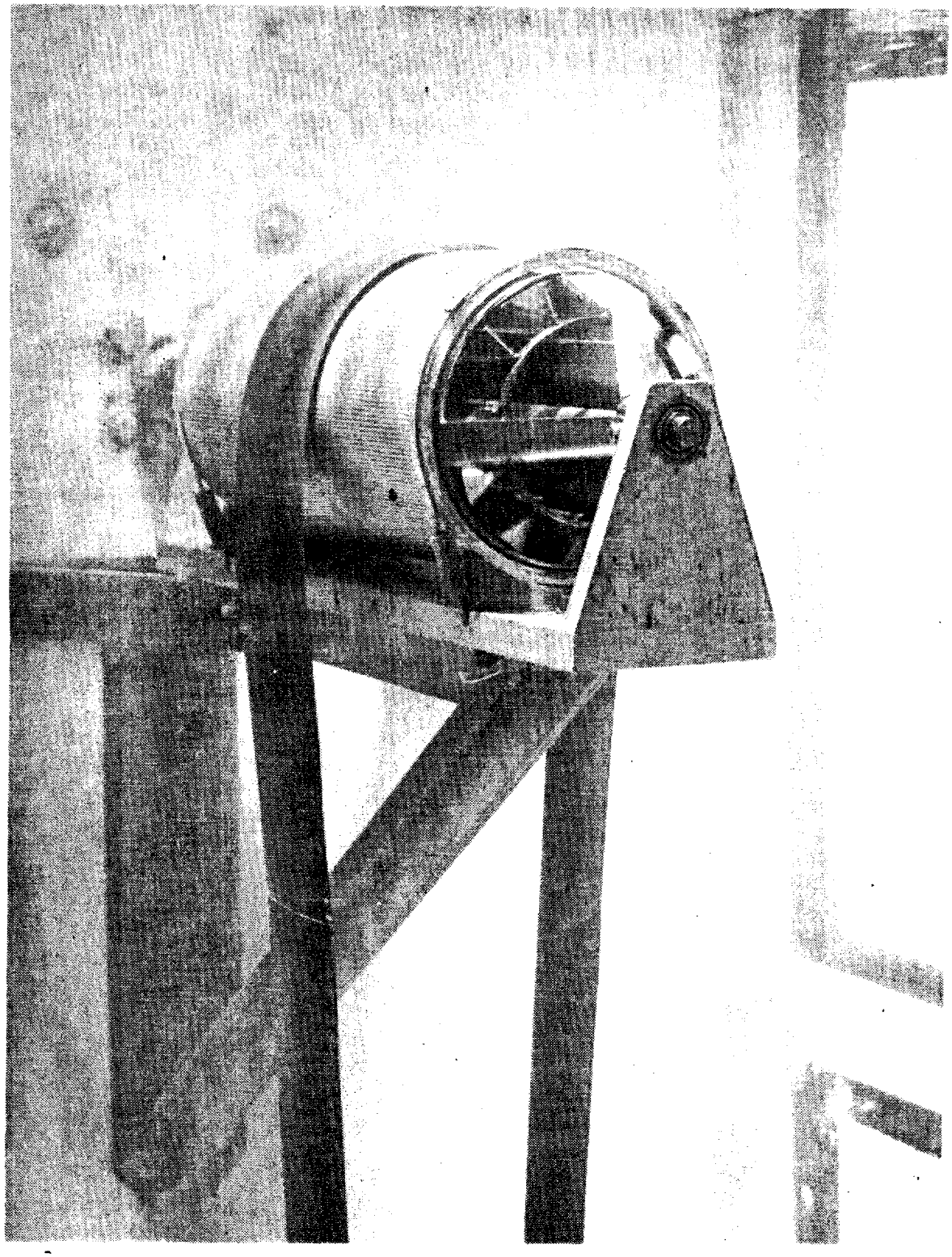

Figure 14. Bearing With Perforated Cage

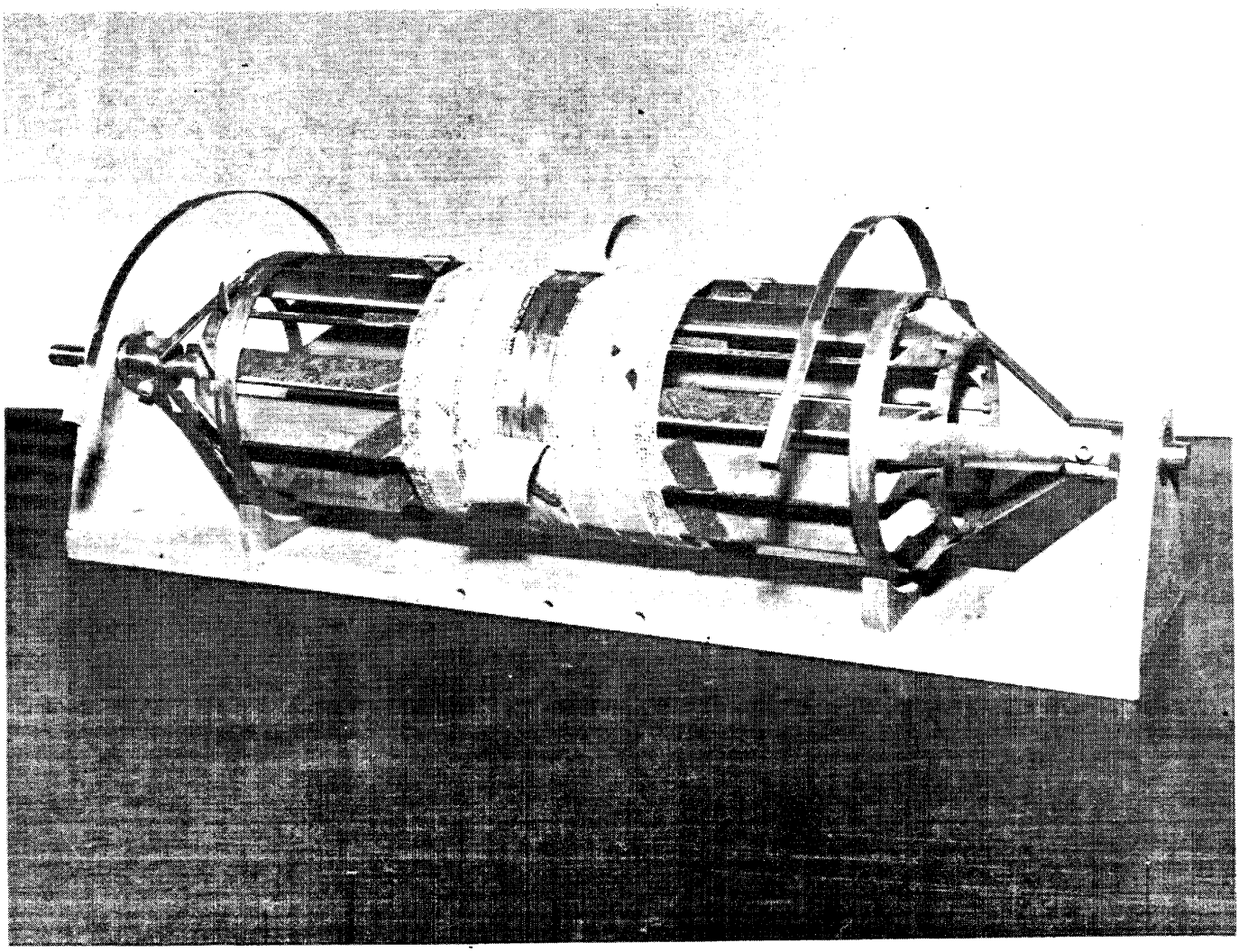

Figure 15. Modification to Impeller Wire Winding

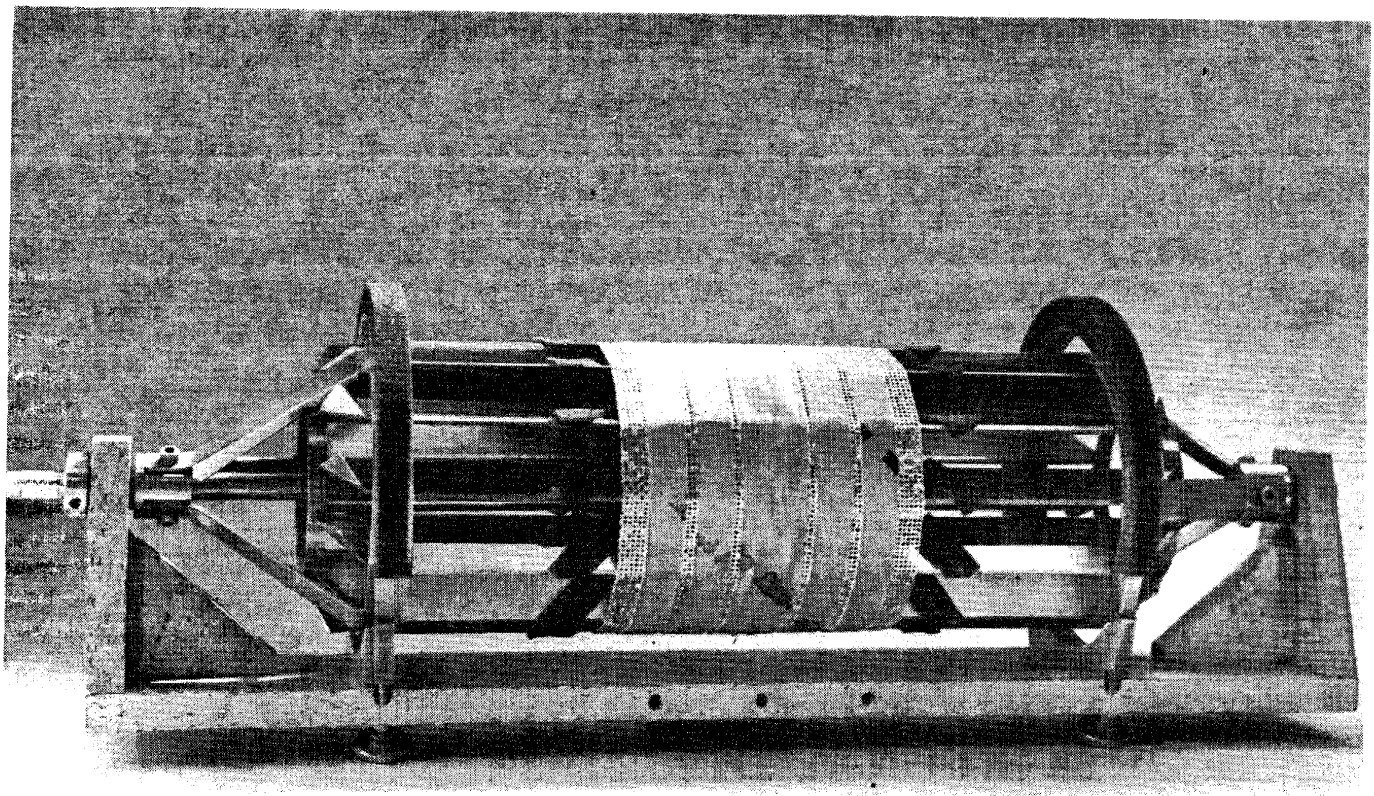

Figure 16. Modification to Drawer Pulley Wheel

Approved For Release 2001/09/03 : CIA-RDP78B04747A002800050001-6

experiments conducted to analyse impeller performance and requirements, consisted of the addition of deflectors (Figure 16) on the impeller blades at an angle of 45 degrees each side of the center disc, to divert a percentage of the fluid flow to the outer ends of the cage, and the blocking off of the lower right-hand portion of the bearing as described for the acrylic plastic slotted cage. Various methods of blocking and restricting the flow on the left-hand side of the bearing similar to Figure 11, Sketch D, were also tested.

With these modifications to the impeller and an overall increase in rpm, a stable cushion was obtained with satisfactory self-centering tendencies.

TABLE 1 - Comparison of Supported Weight Versus RPM & Cushion Height

Film Width	RPM	Wet Weight Load(lbs.)	Cushion Height (Inches)	Stability	Concentricity	Centering
9-1/2-Ins.	342	4.7	1/8	Good	Good	Good
	297	3.5	1/8 - 5/32	Good	Good	Acceptable
6.6-Ins.	342	4.3	1/8	Good	Good	Good
	297	3.25	1/8 - 5/32	Good	Good	Good
5-Ins.	342	2.7	1/8	Good	Good	Good
70m/m	342	0.68	3/32 - 5/32	Good	Good	Good
	272	0.42	3/32 - 3/16	Good	Fair	Acceptable

4. PHOTOGRAPHIC INTEGRITY EVALUATION

The prime purpose of a liquid bearing is to provide a virtually frictionless surface over which photographic film can be transported with a minimum of tension, and without fear of mechanical damage (Figure 17). Whilst the experimental design and testing described in this report were based on determining these requirements, an equally if not more important criterion exists, namely, that the hydrodynamic function of the bearing must not

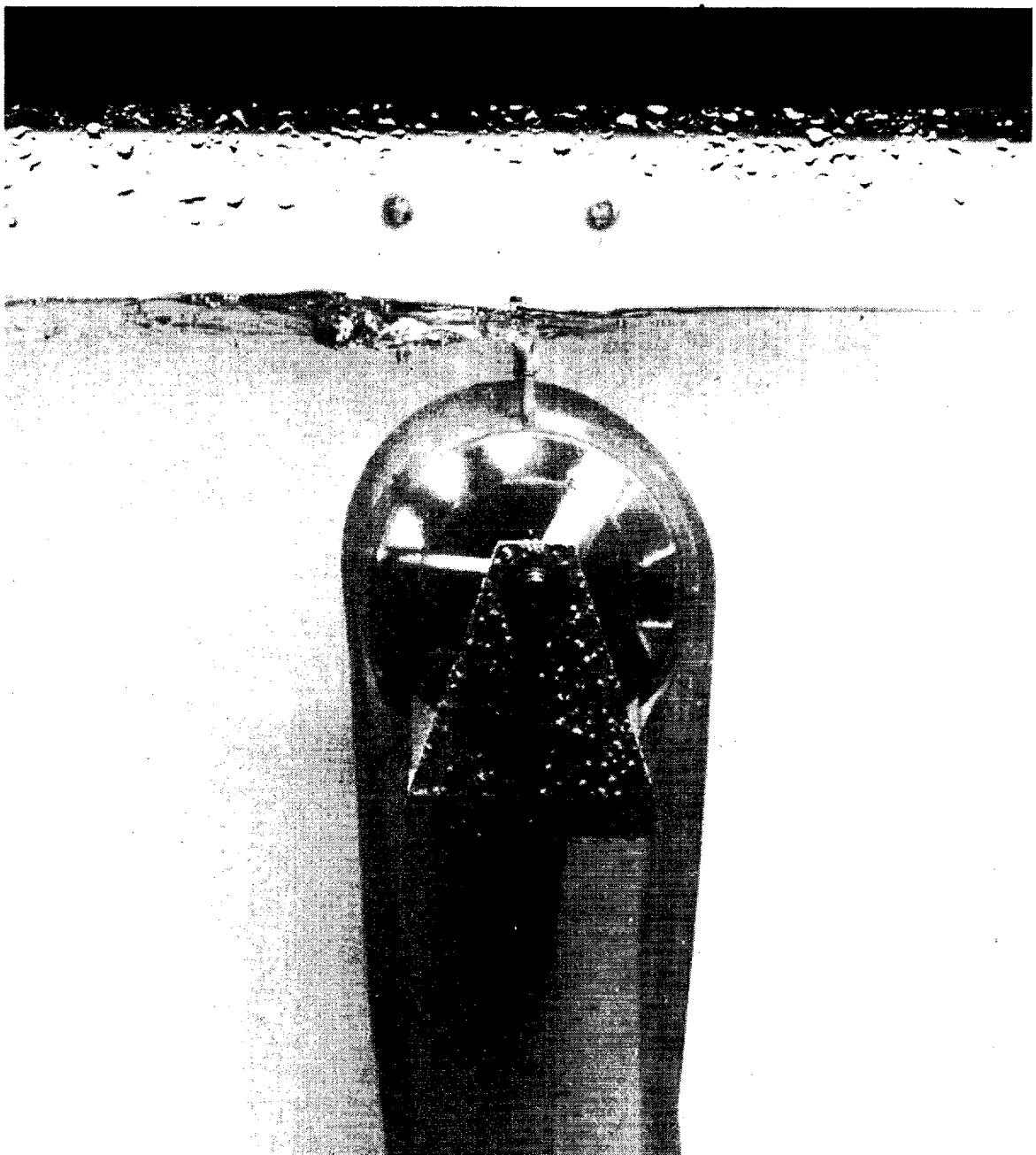

4.1. TEST PROCEDURE

4.1.1. Test Objectives.

The photographic tests were performed to determine the edge-to-edge uniformity of development as a function of the developer turbulance or agitation produced by the Rotatron liquid bearing. The first test was processing of exposed film under controlled conditions. The level of solution agitation in a conventional processor is relatively low in comparison to that with liquid bearings, and this test while determining uniformity of development, also provided data to determine a relationship between the two systems.

The second test was made by the processing of exposed film under adverse conditions by simulating a mechanical failure in a film transport system. The film selected for these tests was Kodak Finegrain Aerial Duplicating film type 8430, processed in the manufacturer's recommended DK50 developer.

4.1.2. Test Set-Up.

The tank used for processing of the test film was the tank used for experimental running of the bearing (Figure 18). Additional rollers were fitted to permit the film to be threaded over the bearing from a standard type A9 magazine. A suitable stop bath and fix tray were also provided, Figure 19.

4.1.3. Film Sample Preparation.

Samples of 9-1/2-inch wide, Type 8430 film, were cut into 10-foot lengths and normally exposed with a point light source, controlled by a variable transformer and timer to provide even intensity of exposure across the surface of the film.

To ensure stabilization of the latent image, the film was encased in a film can in a controlled temperature environment of 71°F. and allowed to age for a four-hour period before processing. The entire processing procedure was completed within eight hours of exposure.

4.1.4. Controlled Test #1.

The film sample was processed over the liquid bearing at a controlled speed of 5 fpm for a period of exactly two minutes at a developer temperature of 71°F. Special attention was given to maintaining the

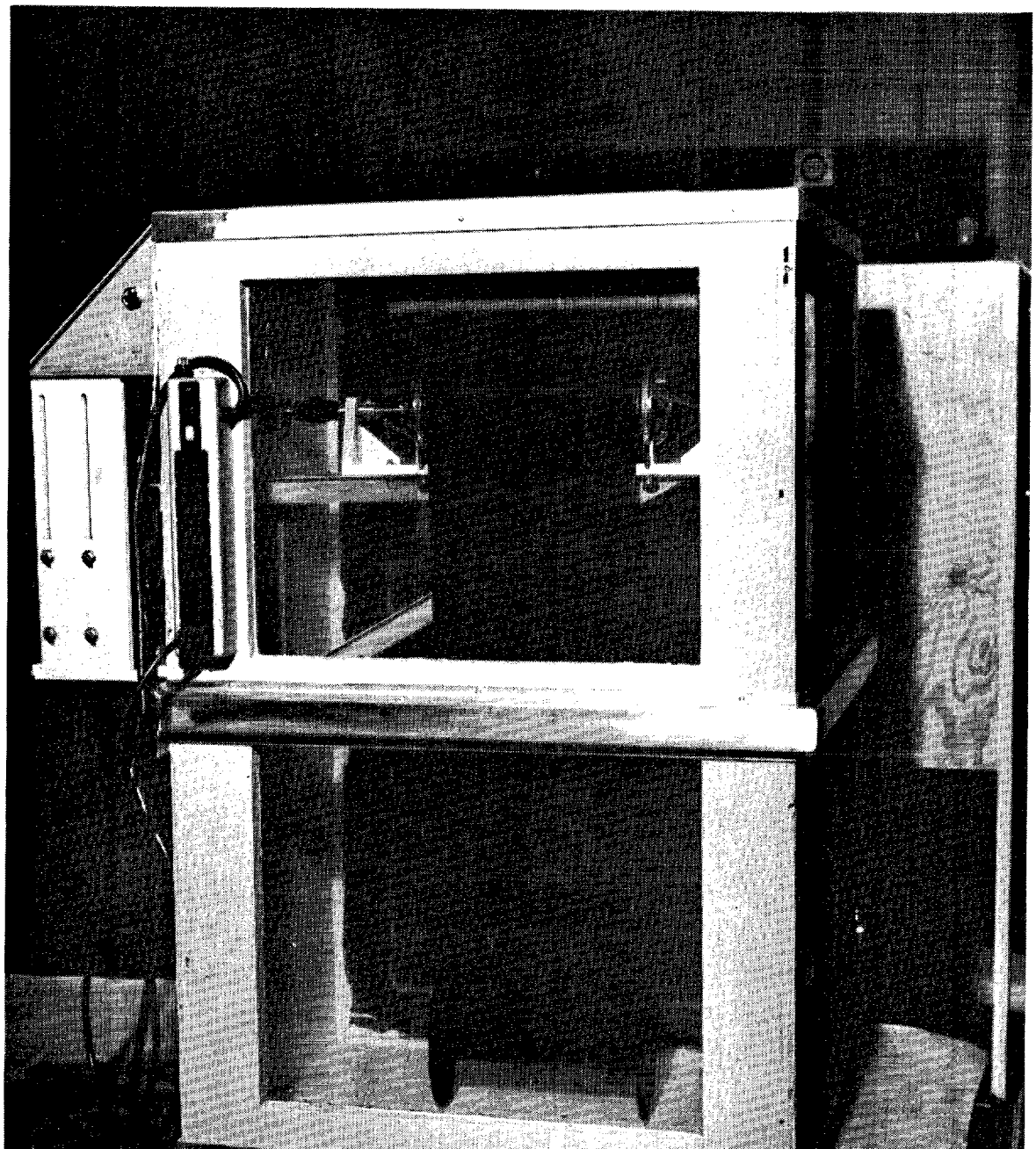

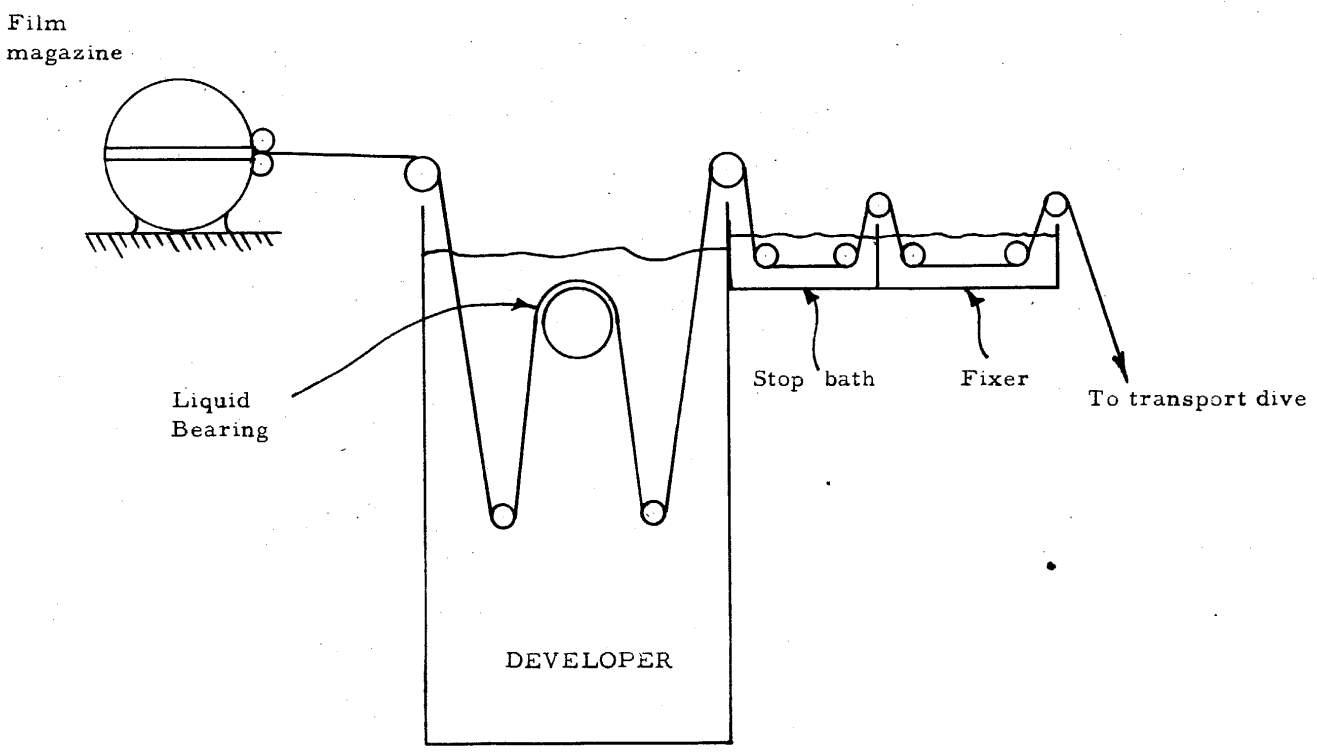

974-013-2

Figure 19 Threading arrangement - photographic integrity tests.

development cycle, the transport system was stopped for a two-minute period and a film loop permitted to form above the bearing. The loop formed from a minimum height of 1/8-inch to a maximum height of five inches above the bearing, and was encouraged to oscillate freely about the bearing. The total processing time under these conditions was four-minutes at 71°F. The transport speed was also varied with sudden stops and starts.

4.1.6. Test Results.
Test #1
The density variation was measured end-to-end on a three-foot length of the sample. The maximum density difference was 0.06, as measured on a Welch "Densichron" densitometer. The maximum edge-to-edge density variation was 0.01.

Test #2
The end-to-end density variation was measured as 0.33. The readings were taken over a length of the sample in which the results of sudden stops and starts in the transport system were most apparent. The maximum edge-to-edge density variation was 0.07, read in the area of the film loop while it was oscillating over the bearing, for the two-minute period of time.

4.1.7. Conclusions and Summary.
Evaluation of the test results indicate that uniform development within extremely close tolerance can be obtained with the Rotatron bearing even under adverse conditions.

It is of interest to note that, during the two-minute period that the free loop oscillated over the bearing in Test #2, the increase in density was negligible. With the film moving about the bearing from a normal 1/8-inch cushion to a maximum free loop of five-inches, the bearing loses its impingement action, and thereby reduces its ability to break-up the laminar layer of exhausted developer by-products on the surface of the emulsion. This effect is considered to have counter-balanced to some degree the increased development time in this localized area of the sample, by decreasing the rate of development in the same area.

5. SUMMARY OF PERFORMANCE

5.1. THE ROTATRON BEARING COMPLETE

The objective of this research program, was to determine the feasibility of a liquid bearing concept, based on the incorporation of the primary source of energy within the bearing itself. Many concepts were considered, but the final decision was given to the design and construction of a bearing which was essentially a conventional twelve-bladed, double-ended squirrel cage, axial-vane pump, rigidly supported and provided with a housing or cage of suitable configuration.

In pressure-plenum type liquid bearings, the primary energy source is obtained from a separate centrifigual pump, located remotely from the bearing or bearings it serves, with the consequent loss in energy in the connecting pipes and hardware. (Reference [redacted] Report 974-001). A further disadvantage is that, to maintain a satisfactory cushion for a range of film widths from 70mm to 9-1/2-inches, edge flanges are required to restrict the loss of fluid from the annular space between the film and the bearing surface. A means of conserving energy is also required when narrower widths of film are transported i.e. if 70mm film is being transported, the loss of fluid through the slots or holes outside of this width, which are necessary for the support of wider films, must be closed.

STATINTL

The main problems encountered during testing of the bearing, was control over cushion depth and concentricity, and retention of the film in the center of the bearing without the use of edge flanges. Four designs of cages were evaluated. Flow of solution in the direction of rotation was determined to be the prime cause of loss of concentricity of the film around the bearing surface. To effect centering of the film, changes to the impeller were necessary to provide a valley profile to the film support cushion rather than the designed-for crown.

Tests proved that no mechanical means of closing the bearing to suit the width of the film was necessary in order to conserve loss of energy. Greater cushion stability with 9-1/2-inch wide film, however, was obtained when a small fixed barrier was provided at each end of the bearing. The results of the evaluation program on the experimental bearing can be extended into an idealized design, a concept of which is discussed in Section 5.2.4.

5.2. IMPELLER PERFORMANCE

The performance of the double ended, twelve blade impeller (Reference Appendix A) was proven to be relatively efficient in that the volume delivery varied directly as the square of the velocity. The velocity pressure was greatest in the central area, falling off towards both intake ends. Axial impellers of this type are generally designed with a L/D ratio of approximately 0.6., but for use within the bearing configuration an L/D of 1.25 was considered necessary to provide a higher pressure and volume near the center to create a "crown" profile. Early tests, however, proved this reasoning incorrect, the fluid crown had the opposite effect, causing the film to slide off rather than be retained in the center of the bearing.

Later testing was concentrated on determining methods of changing the impeller performance characteristics to provide a "valley" profile in lieu of the "crown." The design requirements of the impeller based on the results are discussed in Appendix C.

5.2.1. Evaluation of Cage Performance.
Four types of cages were tested, the first cage was comprised of two oppositely wire-wound helixes. Two types of slotted cages were tested, and a final test made with a cage consisting basically of perforated sheet metal.

5.2.2. The Helix Cage.
The helix cage, as described fully elsewhere, was designed to provide a converging fluid flow, to center the film. The purpose of the stainless steel plate around approximately 120 degrees of the cage was to provide a degree of deflection of the fluid, the cage being rotable in its cradle mounting. The deflection of the fluid by rotation of the cage provided a means of obtaining cushion symmetry. Optimum control was reached at approximately fifteen degrees counter clockwise from the normal position of the plate (lower 180 degree segment). With the impeller rotation clockwise, the plate position reduced the tendency of the film being sucked in at the 4 to 5 o'clock stations. This negative area, the results of fluid flow around the outside of the cage, was proved to exist with other cage configurations. In summation, the influence of the helix pitch on the fluid flow path was negligible, the cage serving only as a cover for the impeller blades.

5.2.3. Slotted Cages.
Two forms of slotted cages were tested, each consisted of a plastic tube in which twenty-four evenly spaced slots were provided. An island was left in the center of each alternate slot to decrease the pressure build-up in the center. Tests showed that control of cushion symmetry and stability were extremely difficult with this type of cage, and that even though a tapered closing of the slots was obtained in the center by the installation of a clamp around the cage, satisfactory centering of the film was not obtained. On the basis of these results, further evaluation tests were not carried out.

5.2.4. The Perforated Cage.
Final test made with support cages (curtailed due to the allocation of manpower effort on higher priority projects), was the evaluation of a 4-1/2-inch diameter perforated screen cage. The fluid cushion produced was very even and stable, with a crown in the center of approximately 3/8-inch in depth. A comparison of the flow through the perforated screen cage and the helix cage, reveals that, with the perforated screen, the plenum pressure gradient was higher at the center and passed a proportionally greater amount of fluid through the screen. The amount dimished towards the ends, thus creating the smooth crown or barrel-shaped profile (Figure 20, Sketch A). In the case of the helix cage, the velocity pressure was delivered direct from the impeller blades with little or no restraint, producing the pressure profile shown in Figure 20, Sketch B. With the helix cage, reshaping of the profile was accomplished by the fitting of a girdle around the outside of the cage.

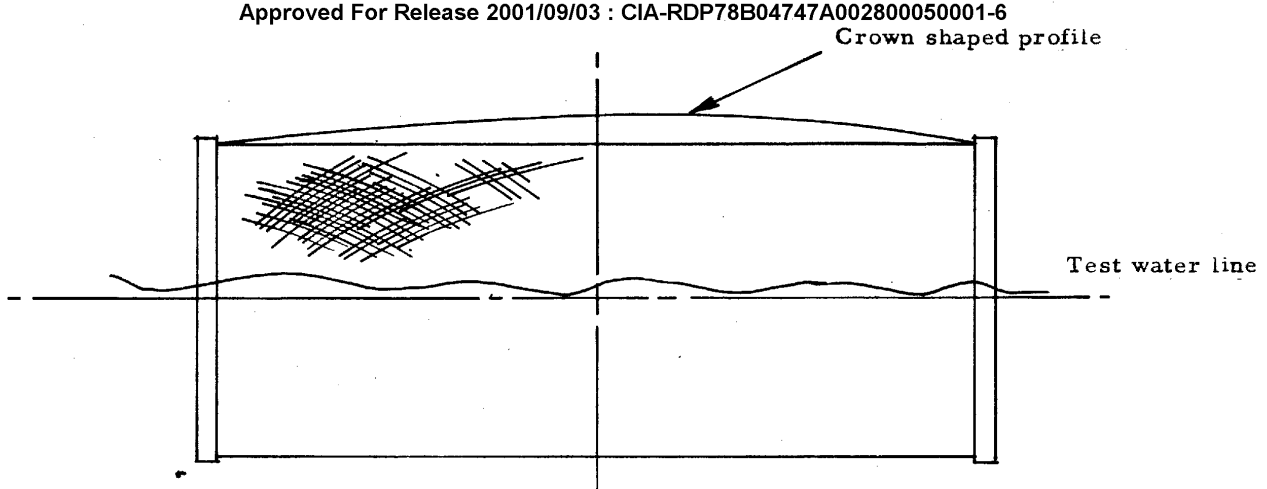

Sketch 'A'
Showing "crown" shaped profile with perforated cage.

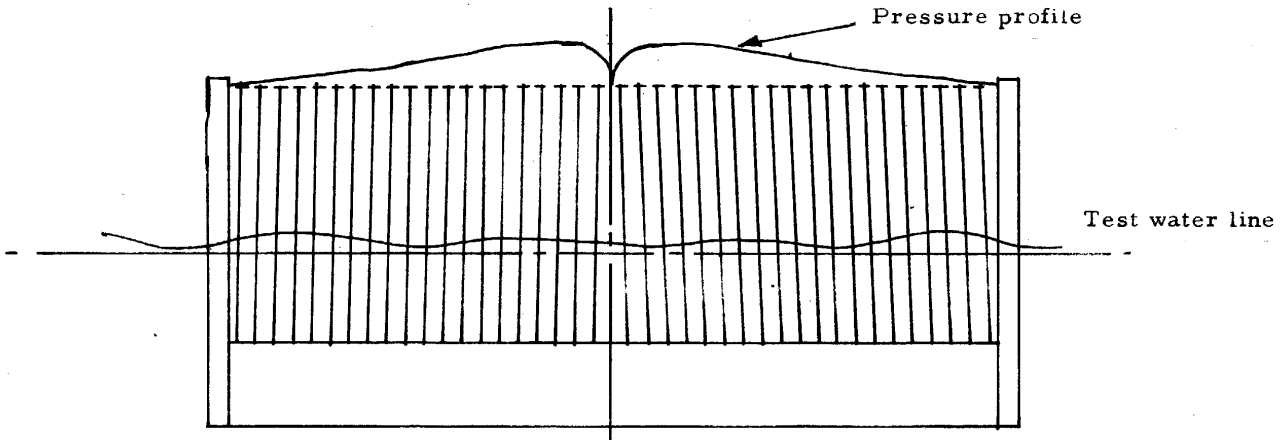

Sketch 'B'
Showing profile obtained with "helix cage
Figure 20 Cage effect on pressure profiles

With the perforated cage, it was decided to determine if the profile shape could be accomplished as an impeller function. With this in mind various degrees of wrapping was placed around the impeller in the area of the higher Pv delivery. The desired improvements in pressure profile were obtained, although the restrictions necessitated an increase in impeller speed to support comparable weights. Fluid flow around the outside of the cage in the direction of impeller rotation resulted in deformation of the film loop. (Reference Figure 11). Measures necessary to restore concentricity of the film loop to the bearing surface included elimination of fluid flow in a clockwise direction under the bearing, and restriction of flow on the left-hand side of the bearing.

The 9-1/2-, 6.6-, and 5-inch films tracked (centered) well on the modified profile while supporting significant loads with a controlled cushion depth of 1/8-inch.

Example:

Impeller speed of 297 rpm.

9-1/2-inch film	-	3.50 pound load
6.6-inch film	-	3.25 pound load
5-inch film	-	2.24 pound load

Separate tests were necessary to obtain impeller changes that would center 70mm wide film while still producing sufficient pressure to provide a stable cushion for this and other films. (Figure 21). With a 1/8-inch cushion depth, the following relationship to the other film widths was obtained.

Example:

Impeller speed of 342 prm.

9-1/2-inch	-	4.70 pound load
6.6-inch	-	4.30 pound load
5-inch	-	2.70 pound load
70mm	-	0.68 pound load

In summary, the perforated screen type cage in conjunction with the impeller modifications provided the most efficient performance. The changes found necessary can easily be incorporated in a finalized design, as shown in Figure 22.

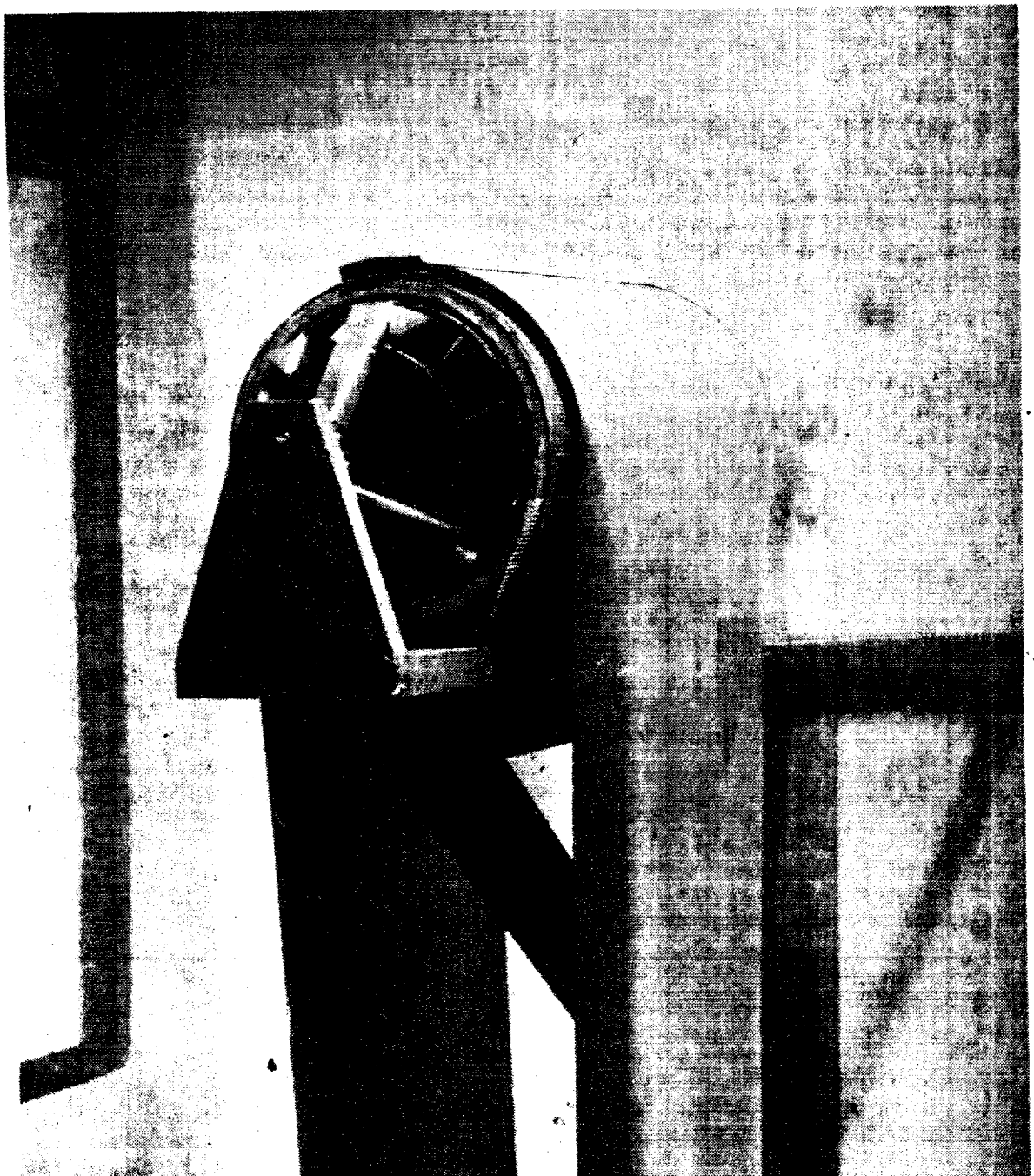

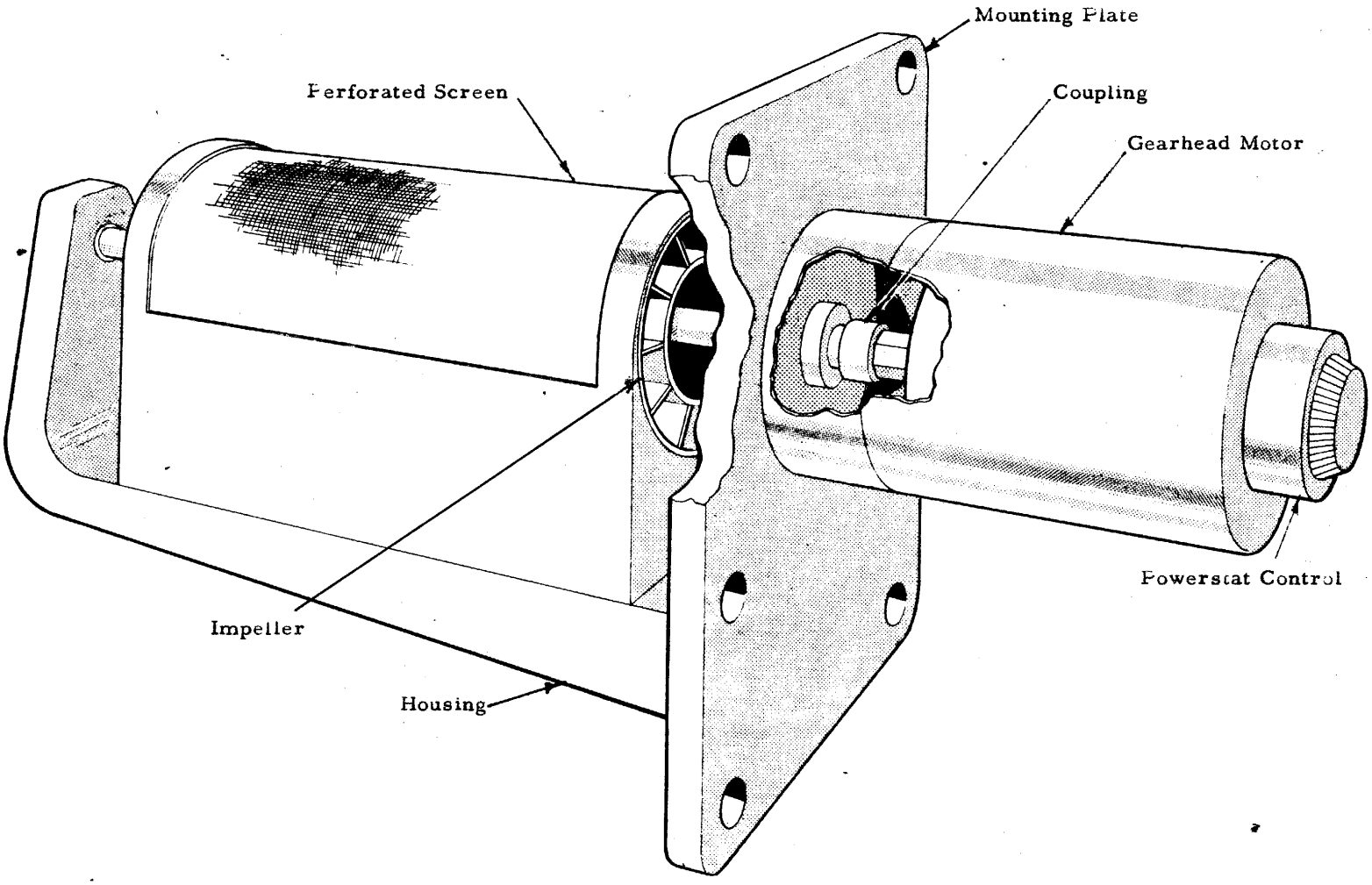

Figure 22. Design Concept of Modular Rotatron Liquid Bearing

APPENDIX A

BEARING LOADS AND DESIGN PARAMETERS

BEARING LOADS AND DESIGN PARAMETERS

1. Pressure Versus RPM

Theoretically, hydraulic pressure varies as the square of the velocity. Stated in simpler words, it takes 4 times as much pressure to deliver 2 times the volume. Examination of the pressure plots read at various speeds indicate that the pressure does vary as the square of the rpm. This fact also means that the flow (gpm) varies directly as the impeller velocity. This would indicate a relatively high efficiency for this particular design.

2. Horsepower Requirements

Theoretically, hydraulic horsepower is calculated on the basis of quantity of flow multiplied by pressure:

$$\text{gpm} \times \text{psi} = \text{hp} \quad (1.71 \text{ gpm} \times 1000 \text{ psi} = 1 \text{ hp})$$

therefore

$$\frac{\text{gpm} \times \text{psi}}{1.71 \times 10^3} = \text{hp}$$

3. Pumping Capability

To evaluate the horsepower requirements of the Rotatron bearing, a test was run to determine the fluid pumped at the various rpm at which pressure readings were made. To accomplish this, a plastic tube (Figure 9) of the same outside diameter as the bearing was placed over the impeller. A smaller tube led the flow of fluid through the side of the test tank to a standpipe, establishing a hydraulic head equal to that in the tank. Water was supplied to the tank through a flowmeter at a rate sufficient to maintain the established head above the bearing. A pressure probe was inserted in the plastic tube surrounding the impeller. Another probe was inserted in the outlet tube to read the back pressure in the outlet line. The difference between the pressure readings would

4. Measured Volume Flow

The gallons per minute and the pounds per square inch at various rpm are given in Table A1.

Examination of average psi readings reduced from pressure plots combined with the flow rates at the corresponding rpm, show that the hydraulics horsepower requirements are extremely low. It should be noted again here, that the flow varies with the velocity and the pressure varies as the square of the velocity.

TABLE A1

GALLONS PER MINUTE AND
POUNDS PER SQUARE INCH
AT VARIOUS RPM

RPM	GPM	PSI
296	9.35	0.098
356	11.3	0.141
467	14.7	0.243

applying the horsepower formula, $\frac{\text{gpm x psi}}{1.71 \times 10^3} = \text{hp}$:

at 296 rpm, $\frac{9.35 \times 0.098}{1.71 \times 10^3} = 0.00055$ hp

at 356 rpm, $\frac{11.3 \times 0.141}{1.71 \times 10^3} = 0.000933$ hp

at 467 rpm, $\frac{14.7 \times 0.243}{1.71 \times 10^3} = 0.00209$ hp

be proportional to the load requirements. The pressure required for a given load, based upon the actual load (spool weight) during rpm runs, is consistent with the psi over a projected area of the film. To put it more understandably, so many pounds per square inch multiplied by the number of square inches of the film over the bearing approximates very closely the weight of the spool. By the same token, the increase in rpm required to maintain the same cushion depth (approximately) with a heavier load on the spool is very consistent with the psi generated by the rpm increase.

Assume that the weight of the spool in the test loop was doubled. This would require twice the psi to maintain the desired cushion. If the pressure increase is 2, the speed increase must vary as the square root of 2, or 1.414.

For example: say the original rpm is 150 and the psi is 1.5. The new pressure required is 3.0 psi:

$$\left(\frac{1.414 \times 150}{150} \right)^2 = \frac{X}{1.5}$$

$$\left(\frac{210}{150} \right)^2 = \frac{X}{1.5}$$

$$(1.414)^2 = \frac{X}{1.5}$$

$$2 = \frac{X}{1.5}$$

$$X = 2 \times 1.5 = 3.0 \text{ psi}$$

6. Rotatron Design Parameters

Bearing Diameter. The diameter of the experimental Rotatron bearing was chosen as an optimum size based upon the force required to bend film

Impeller. The number of impeller blades (12) was chosen to give a space between each approximately equal to the blade chord (width). (See Figure 1.) This proportion is in keeping with optimum design criteria generally used in pumps and fans of this type. The blade width was a function of the frontal area exposed at the angle of attack (45 degrees to the tangent at the blade leading edge). Each blade was assumed to be doing a fraction of pumping equivalent to the number of blades, that is, 10 blades at 10 percent, or 12 blades at 8.33 percent; in effect, 1 blade at 100 percent.

For example:

Rotatron blade width = 0.75 inch

12 blades at 8.33 percent = 1 at 100 percent

effective blade length = 10-inches.

$$\text{Pumping capacity} = \frac{A \times B \times \text{rpm}}{C} = Q$$

where

A = blade width

B = effective blade length

C = 231 (cubic inches per gallon)

Q = gpm.

It has been stated that the pumping efficiency of the Rotatron is relatively high. Here is a comparison of the theoretical and actual output based upon the above formula.

$$\text{For 296 rpm:} \quad \frac{0.75 \times 10 \times 296}{231} = 9.6 \text{ gpm}$$

For 356 rpm: $\frac{0.75 \times 10 \times 356}{231} = 11.55$ gpm

Actual test reading was 11.3 gpm

For 467 rpm: $\frac{0.75 \times 10 \times 467}{231} = 15.17$ gpm

Actual test reading was 14.7 gpm

The formula used above is the result of emperical and theoretical data. Inasmuch as the impeller was designed to suit the bearing configuration and is a radical configuration as impellers go, it was not deemed advisable to spend time designing a prototype by more academic methods. The test results indicate that this approach was adequate.

APPENDIX B

MATHEMATICAL ANALYSIS OF THE BEARING PRESSURE FLOW PATTERNS

APPENDIX B

Mathematical Analysis of the Bearing Pressure-Flow Patterns.

Part I

Earlier experimentation in the preceding contract as reflected in Reports 974-003-1 and 974-013-1 ("Hydromatic Liquid Bearing Assessment" and "Designing, Constructing and Testing a Liquid Bearing Incorporating a Built-In Pump") established conclusively that a flow pattern, in which fluid pressure was higher at the edges of the supported film and lower at the center, created a self-centering effect. Similar to the action of a crowned pulley, if the film were manually moved off center, it immediately readjusted to a center tracking position. This uneven, or "bow-tie," flow pattern is subject to theoretical mathematical analysis.

Using Neville's familiar notations for Jacobi's theta functions and substituting L for K, we have:

$$\vartheta_s(u) = \frac{H(u)}{H'(0)} \tag{1}$$

$$\vartheta_c(u) = \frac{H(u+L)}{H(L)} \tag{2}$$

$$\vartheta_d(u) = \frac{\theta(u+L)}{\theta(L)} \tag{3}$$

$$\vartheta_n(u) = \frac{\theta(u)}{\theta(0)} \tag{4}$$

These notations are simplifications of Jacobi's elliptic (or doubly periodic meromorphic) functions in which L and i L' are the quarter periods defined by:

$$L(m) = L = \int_0^{\pi/2} \frac{d\theta}{\sqrt{1 - m \sin^2\theta}} \tag{5}$$

In equations (5) and (6), m (the parameter) and m_1 (the complementary parameter) are any real numbers having the relation $m + m_1 = 1$. Therefore, we may assume $0 \leq m \leq 1$. In equations (1) through (4), the notations s, c, d, and n refer to the points 0, L, L + i L', and i L' respectively, on the Argand diagram. Formulae (1) through (3) are of no concern in this analysis since they are related to the first order sine, cosine, etc. functional variation. The notation, u, is defined similarly to the L integrals:

$$u = \int_0^{\varphi} \frac{d\theta}{(1-m \sin^2 \theta)} 1/2 \qquad (7)$$

Where φ is the amplitude or

$$\varphi = \text{am } u \qquad (8)$$

Again substituting in equation (4):

$$\vartheta_n(u) = \frac{\theta(u)}{\theta(0)} = \frac{\vartheta_4(v)}{\vartheta_4(0)} \qquad (9)$$

In the latter expression, let

$$v = \frac{\pi u}{2L} \qquad (10)$$

Represented graphically, it can be seen

Considering the bearing in cross-sectional side elevation, L represents the length. The effective area of film support (exhibiting self-centering properties), extends from L to 3L, in this case approximately 10 inches. If the minimum lifting pressure at the center is assumed to be unity, then it can be seen that the ratio 1.2:1 at the outer edges is the minimum value operable and still preserve symmetry. This checks closely with observed experimental results.

Obviously, to obtain the total lifting force available for supporting the film, a second integration would have to be performed to 0 to π in a plane perpendicular to the bearing axis. This is beyond the scope of this report, since the theta function is the idealized case, and actual measurements show a point-to-point variation in its profile. The solution would, however, be easily subject to analysis by analog and/or digital computer.

PART II

The balance of the analysis can be made by means of the classical dimensional theory of frictionless flow in outward flow "parallel" vane turbo machinery systems. Certain basic assumptions must be made in order to prevent the mathematics involved from becoming hopelessly unwieldy. These are:

1) The fluid is incompressible and frictionless.

2) In tracing the contour of a force path, the system flow is one of constant energy.

3) Pressure differences do not include gravitational forces - differences in elevation being considered eliminated by measuring all pressures at one elevation.

4) The vorticity of a particle of a frictionless fluid does change with time.

5) The "Joukowski condition," that the flow of a frictionless fluid leaves the trailing edge of a deflecting vane smoothly, obtains.

If a cylindrical section is taken through an axial flow runner such that $U_1 = U_2 = U$ (where the symbol, U, represents the peripheral, or tangential, velocity and the subscripts refer to entrance or exit from the impeller area), the following general equation can be derived:

$$\frac{H}{\eta_h} = C_H (V^*_{U2} - V_{U1}) = \frac{U}{g} = C_H V^*_U \frac{U}{g} \tag{11}$$

in which

H = total head, or static plus velocity head in ft-lbs/lb, or ft.

η_h = hydraulic efficiency.

C_H = head correction factor, dimensionless.

V^*_{U1}, V^*_{U2} = fictitious rotational, or peripheral, components of velocity in ft/sec.

V_{U1} = true effective entrance peripheral velocity in ft/sec.

g = gravitational acceleration in ft/sec.^{2}

Equation (11) is recognized as the classic Euler relationship. Referring to Figure B-2, the relations between entrance and exit velocities may be expressed:

$$V_{U2} - V_{U1} = \Delta V_U = \quad - \Delta v_x \tag{12}$$

Where v_x is the fluid velocity vector of the vane along the x-axis. In the diagram, the direction of rotation was reversed from that actually used in the "Rotatron" to avoid obtuse angles and negative vectors. As developed, the analysis is still valid. If the fictitious value is substituted, the relation becomes:

$$V^*_{U2} - V_{U1} = \Delta V^*_U = - \Delta v_x \tag{13}$$

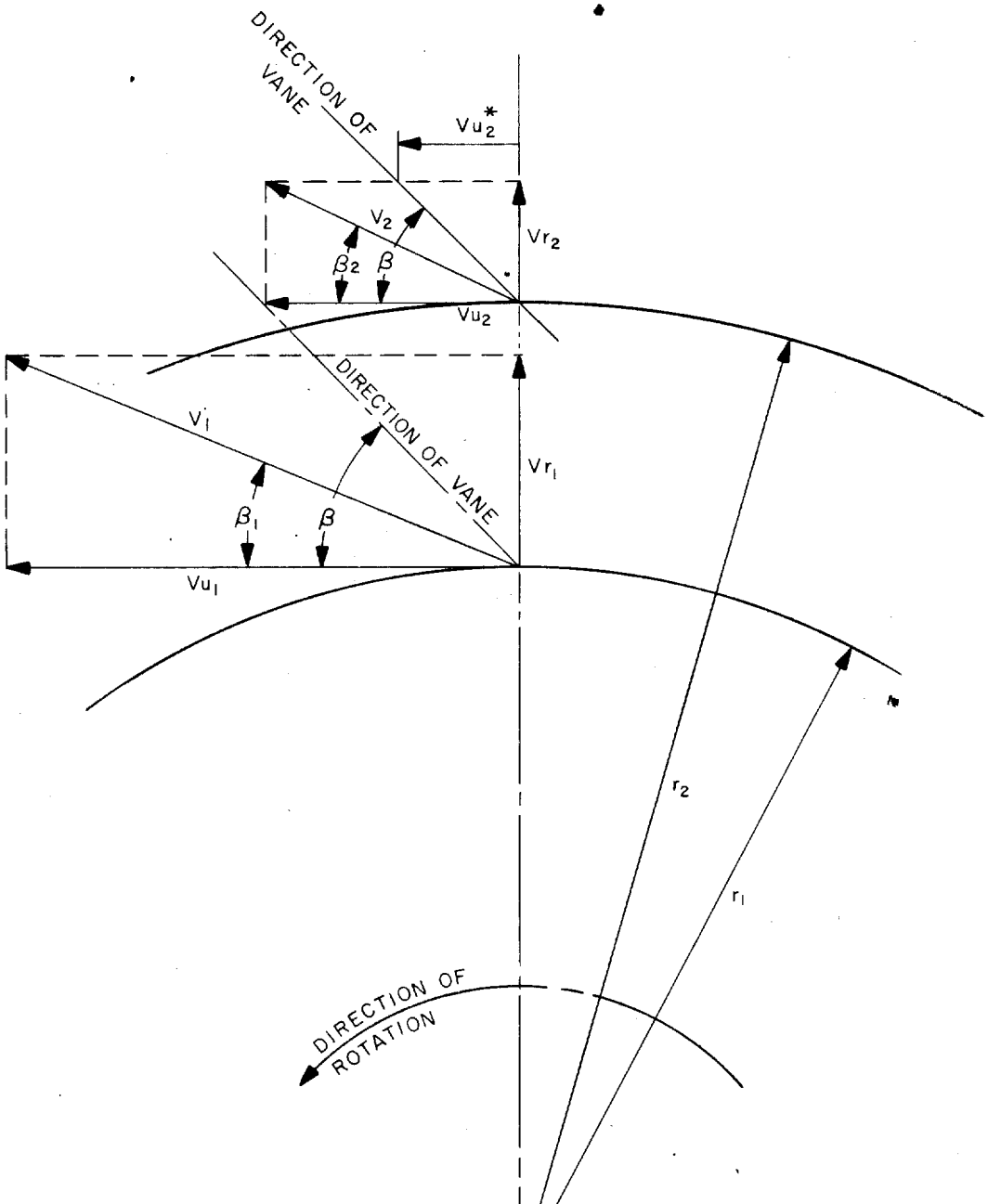

Furthermore, it can be shown that

$$\frac{\Delta v_x}{2} = \frac{\Delta v_x^*}{(t/l)\ (2/\pi K)\ (1/\sin\beta) + 1} \tag{15}$$

where

t = vane spacing, any unit of length

l = vane length, same units as t

K = Weinig's lattice - effect coefficient

β = angle between relative flow and peripheral direction in radian, or degrees

When the value of $\frac{\Delta v_x}{\Delta v_x^*}$ as derived from Equation (15) is integrated

with Equation (14), C_H becomes:

$$C_H = \frac{2}{(t/l)\ (2\pi K)\ (1/\sin\beta) + 1} \tag{16}$$

Values of C_H are shown graphically, Figure B-3, and values of K, Figure B-4. Substituting Rotatron dimensions, the following relationships appear:

$$t/l = \frac{0.712}{0.878} = 0.811 \tag{17}$$

$$\beta = 45^\circ \tag{18}$$

$$C_H = 0.956 \text{ (Figure B-3)} \tag{19}$$

$$K = 0.650 \text{ (Figure B-4)} \tag{20}$$

974-013-2

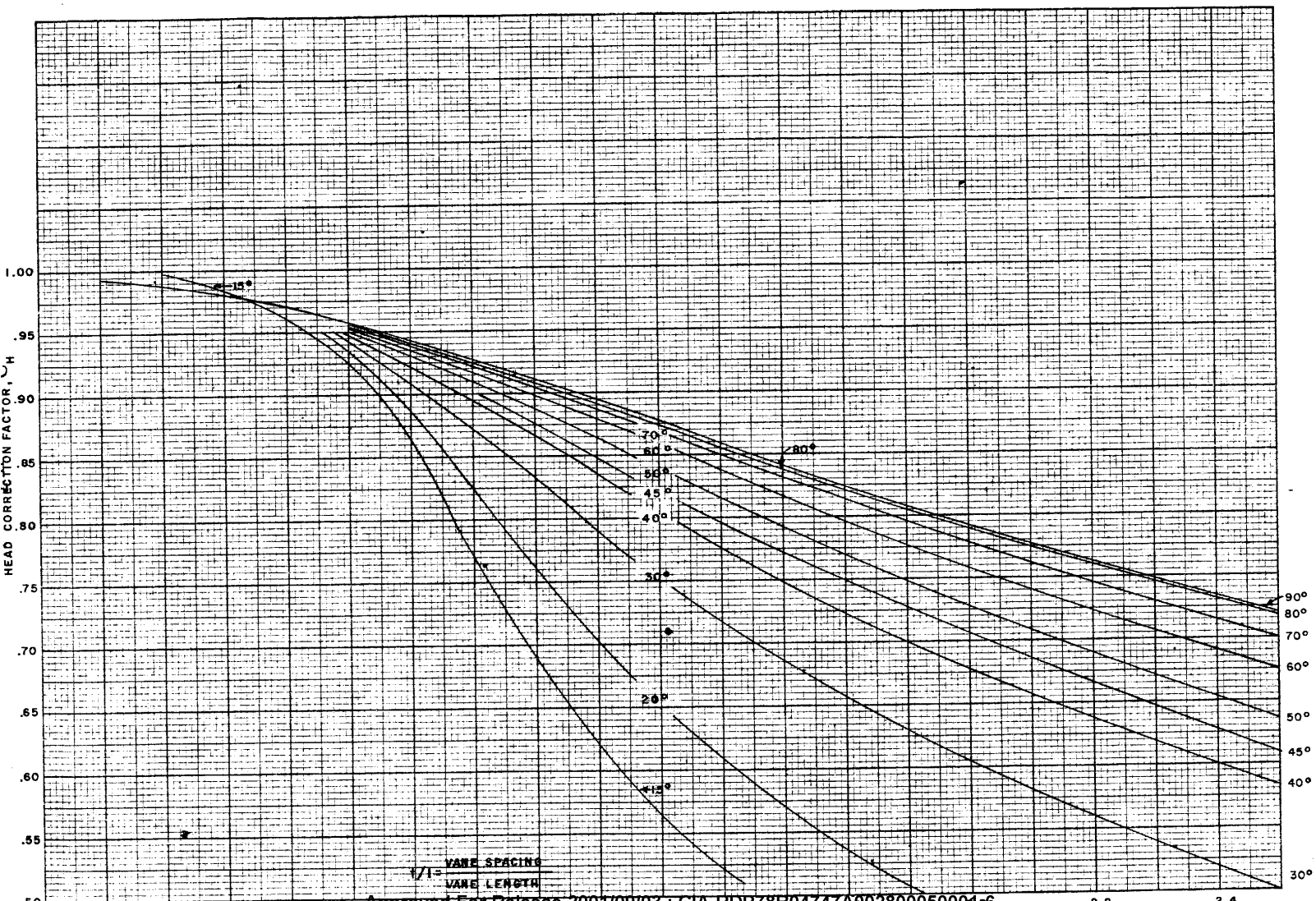

Figure B-3. Head Correction Factor for Axial-Flow Runners

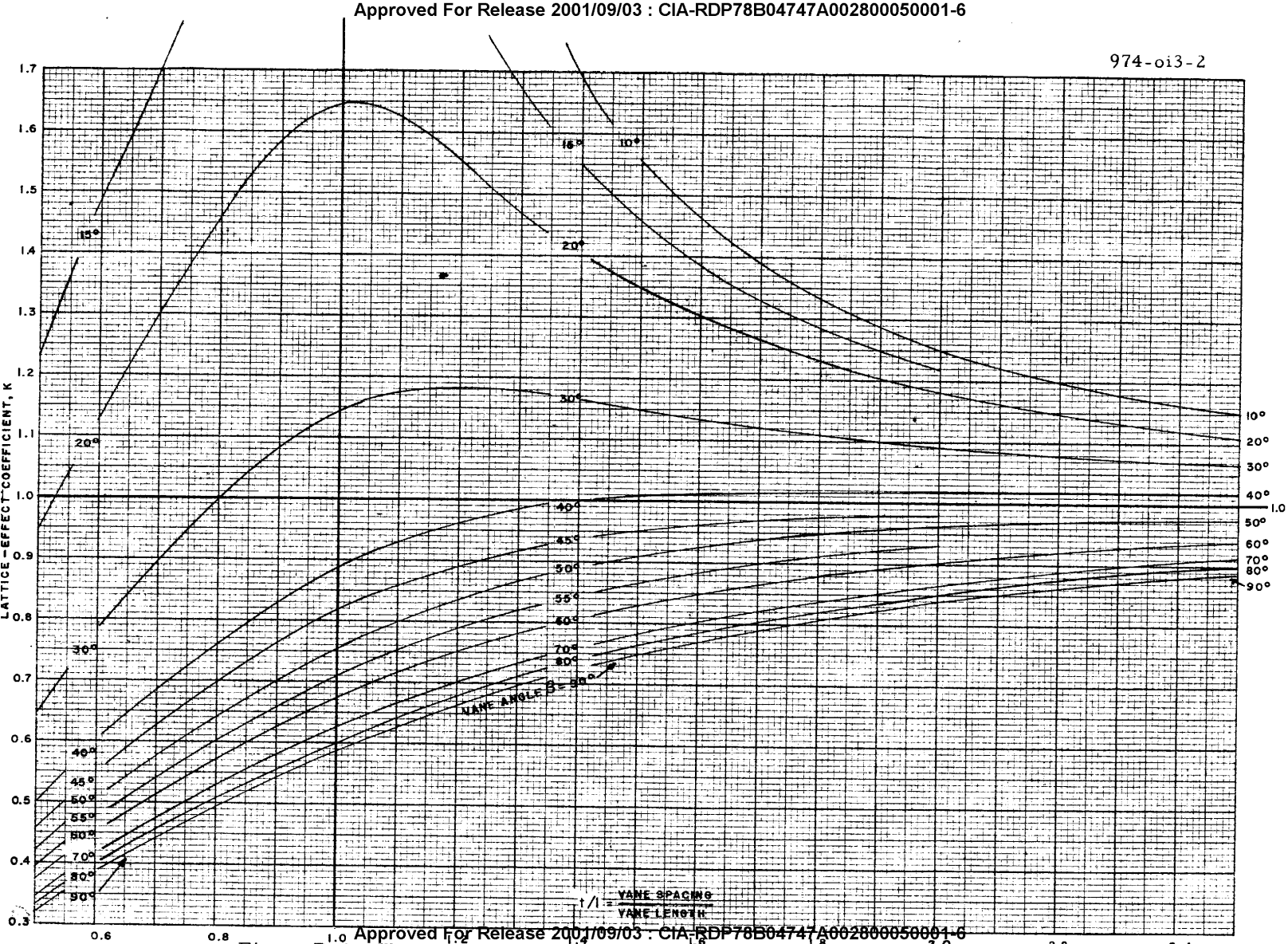

Figure B-4. Weinig Lattice-Effect Coefficient for Frictionless Flow Through Vane Systems

In this case, where the vanes are flat (neglecting a small bend on the inner radius), the angle of attack, α, between the line of zero lift and a line tangential to the intersection of the inner radius, is equal to .

Substituting:

$$C_L = 2\pi K \sin\beta = 2\pi \times 0.650 \times .70711 = 2.89 \qquad (22)$$

Now, by combining Equations (11) and (16), the following derivation for ΔV_U is obtained:

$$\Delta V_U = \frac{U}{1/2 + \frac{(1)}{(\sin\beta)}\,\frac{(t)}{(l)}\,\frac{(1)}{(\pi K)}} \qquad (23)$$

One of the characteristic speeds used in the testing was 296 rpm. This gives a value of U of 4.34 ft/sec. Substituting in Equation (23) shows ΔV_U to be 3.91 ft/sec. The Euler relationship, Equation (11), may be rewritten as:

$$H = \frac{r\omega}{g}\,(V_{U_2} - V_{U_1}) \qquad (24)$$

where

ω = angular velocity in radians per second

$$H = \frac{\frac{1.68}{12} \times \frac{45}{360} \times \frac{296}{60} \times 3.91}{32.17} \qquad (25)$$

$$= 0.105 \text{ ft. of water.}$$

If this figure is translated into lift over the projected area of 9-1/2-inch film, a total axial force of 0.278 pounds per effective vane is obtained, or a total lifting capacity of 3.34 pounds. This figure compares favorably with the actual measured weight of 3.5 pounds, the discrepancy being explained by the fact that the assumed efficiency factor was too low.

APPENDIX C

OPTIMUM IMPELLER DESIGN FOR ROTARY BEARINGS

OPTIMUM IMPELLER DESIGN FOR ROTARY BEARING

Once the experimental results and empirical data have been critically analyzed, the optimization of an efficient impeller design can be formulated. Thus, Figure C2 and C3 illustrate configuration potentials which would produce a desirable cushion when used with a perforated screen cage.

A comparison with Figure C1 (the basic configuration of the test impeller) shows Figure C2 to have blades set so that the inboard and (center) of the blades would be traveling at a slower peripheral speed thus delivering less pressure velocity. For example:

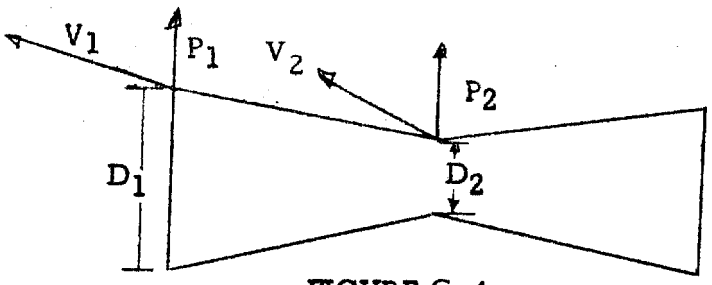

FIGURE C-4

Functional Relationship of angled blade

If $P2_{V_2}$ is set at .85 $P1_{V_1}$ (15 percent less flow), the relationship becomes:

$$\frac{P_1}{P_2} = \frac{V_1^2}{V_2^2} = \frac{D_1{}^2}{D_2{}^2}$$

Solving for D_2 gives $D_2 = D_1 \sqrt{.85} = .922\ D_1$.

A second configuration, similar to Figure C2 would be an axial impeller with diminishing blade width. P_2 would become lower towards the center of the bearing due to diminishing volume flow.

A third type of axial impeller design which could control the cushion shape is one changing the angle of attack, or vane shape. (Figure C3). The logarithmic is recognized as the simplest curve or vane shape for a radial flow system.

Since a line of constant inclination (angle of attack) against the peripheral, or radial, direction is the least complex, it would seem logical to consider primarily the variations of this inclination as a criterion for general vane shapes.

Figure C3 shows a striking example of a vane shape with a simple variation of its inclination against the peripheral direction.

It can be seen that the angle of inclination varies linearly from one end of the vane to the other, this angle being plotted against the distance from the center of the system (from leading edge of blade to trailing edge). If this variation were to cover a fairly wide range (e.g., from 15 to 90 degrees, as shown), the resulting vane shape would have a double curvature. It is clear that it would be possible to construct a vane shape with a single curvature having the prescribed angle B_1 and B_o on both ends but a different form of angular variation between these two extremes. However, the form with the simpler angular variation as shown in the figure comes much closer to the forms actually used for hydrodynamic runners of this type. From this, one may draw the tentative conclusion that the angular variation suggested here is of primary importance, not only geometrically, but also hydrodynamically. On the other hand, it would not be realistic to draw the conclusion that the vane shape shown would be the best for impellers of this type. Such a conclusion can never be drawn on the basis of purely geometric (analytical) considerations. It is to be expected that some departures from the linear variation of the vane angle would be necessary to obtain the best results. The figure is intended to illustrate a certain tendency in the relation between the geometric and the hydraulic design of a radial-flow impeller without making any statement concerning the optimum form of design.

Inasmuch as the <u>total</u> system is important to an optimum impeller design

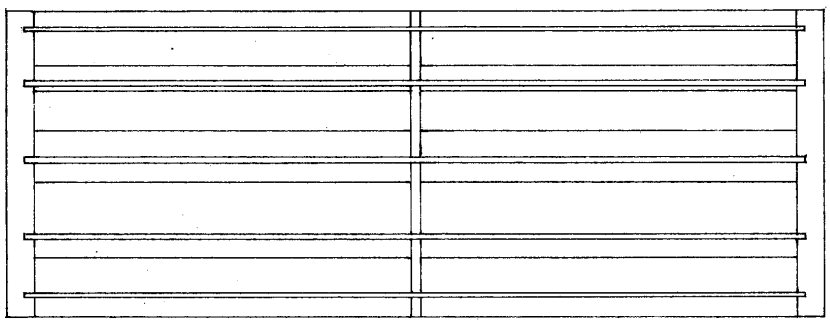

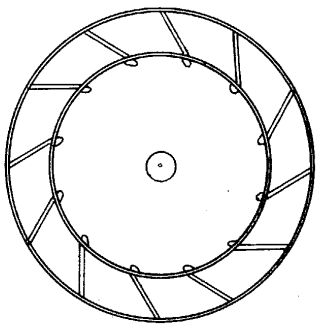

Figure C - 1. Basic Impellor Design

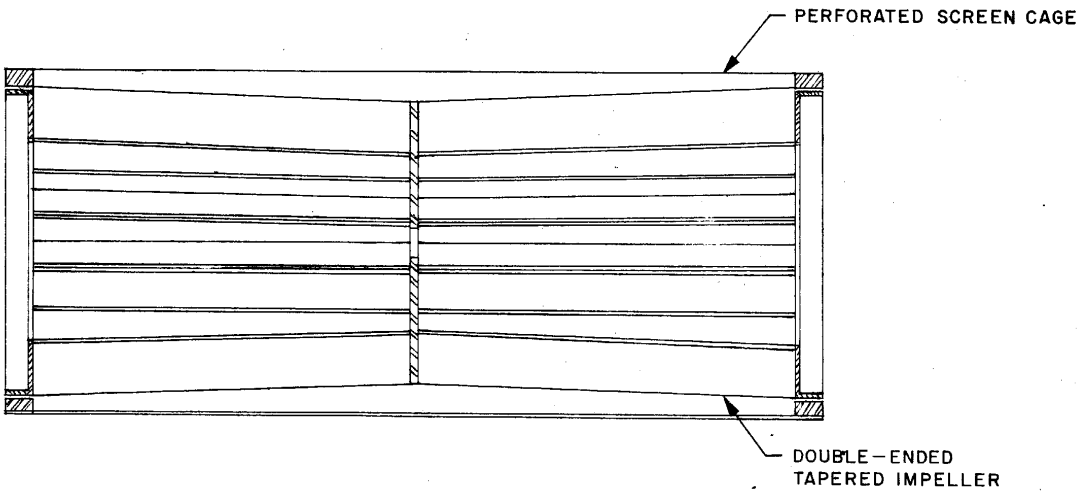

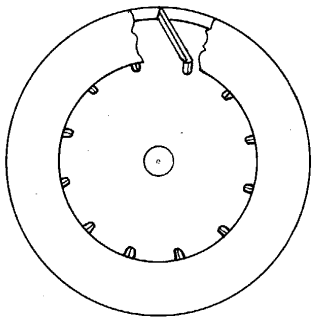

974 - 013 - 2

Figure C - 2 Modified Impeller with Tapered Blades

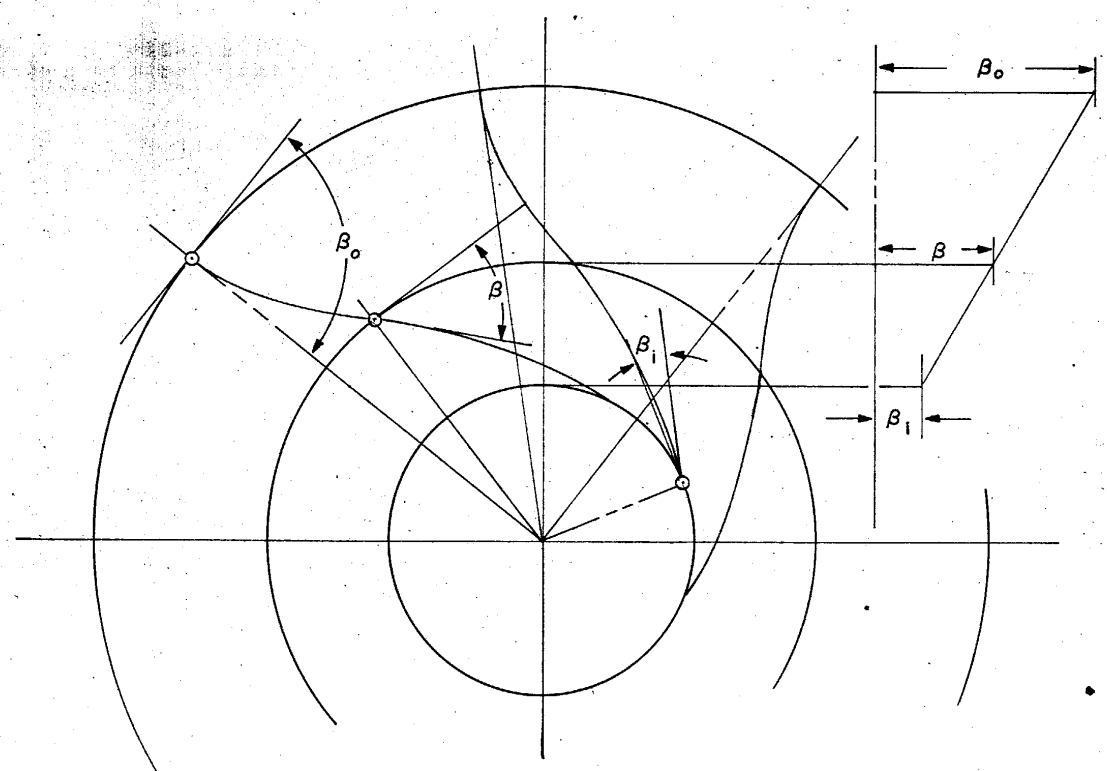

Where $_i$ = 15°, = 45°, o = 90° and = angle of attack

Figure C-3 Variation of Angle of Attack

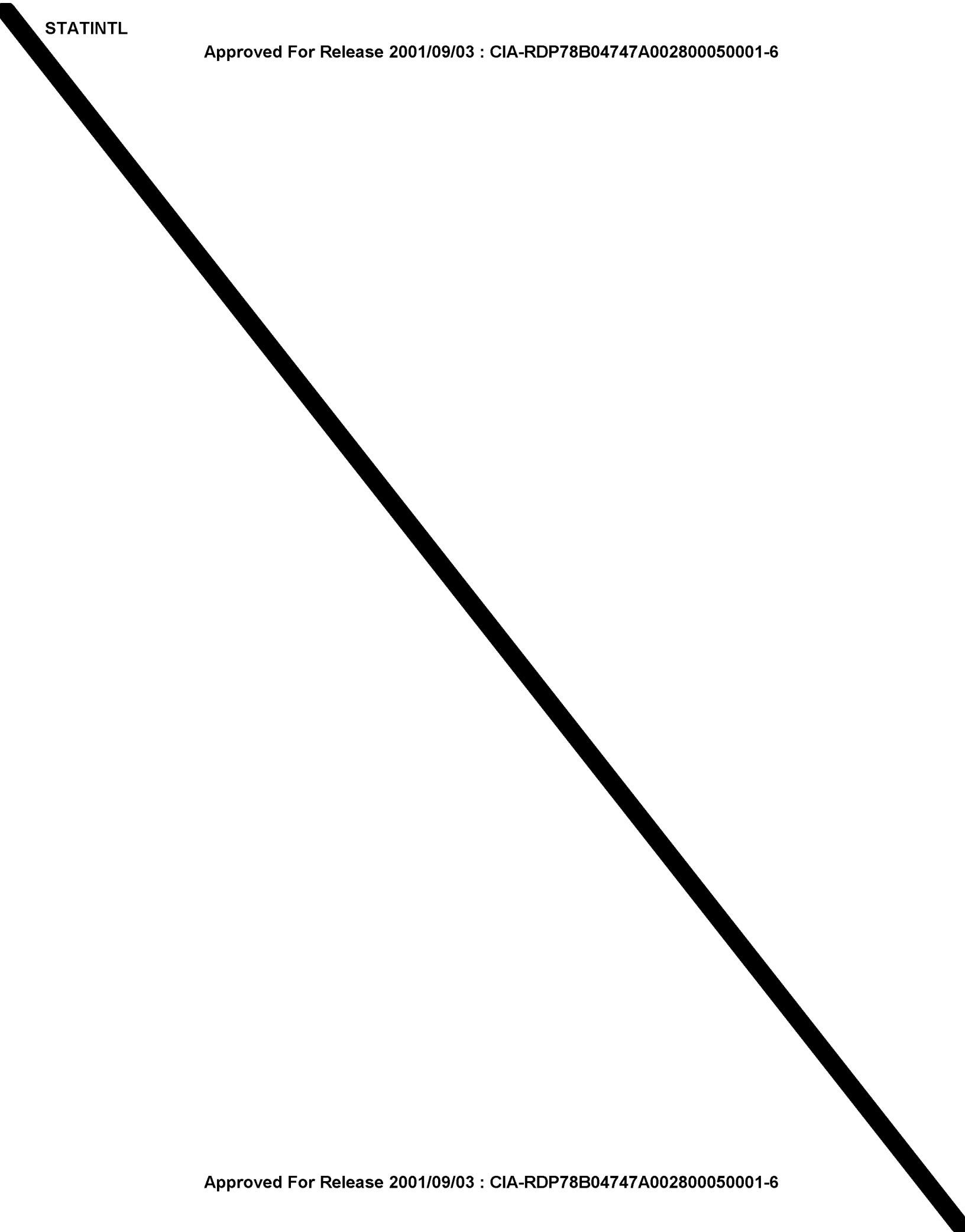

Approved For Release 2001/09/03 : CIA-RDP78B04747A002800050001-6